Mixed Formulation of Inelastic Composite Shear Beam Element

Dipankar Das, S.M.ASCE, [1] and Ashraf Ayoub, PhD, PE, FACI, FASCE[2]

[1]Ph.D. Candidate, School of Mathematics, Computer Science and Engineering, City, University of London, London, U.K.,EC1V 0HB; e-mail: dipankar.das.1@city.ac.uk

[2]Professor, School of Mathematics, Computer Science and Engineering, City, University of London, London, U.K., EC1V 0HB; e-mail: ashraf.ayoub.1@city.ac.uk

ABSTRACT

This study presents a new beam element formulation following a Hellinger-Reissner functional for composite members considering coupling between bond-slip and shear deformations. A robust state determination along with new stability criteria for the mixed-based formulation is proposed. The constitutive laws of the concrete, steel, and shear connectors are used to derive the inelastic coupled axial-flexural-shear interaction of the composite element. To consider shear deformations, a Timoshenko beam theory has been adopted in deriving the section kinematics equations. J2 plasticity following radial return mapping algorithm and fixed crack smeared softened membrane model are used to simulate the multi-axial stress state in steel and concrete respectively. The accuracy and efficiency of the mixed-based formulation was evaluated by comparing the responses at local and global levels with the displacement-based formulation.

INTRODUCTION

In today's engineering practice, it has become imperative to have a robust and reliable numerical model to design new structures and to assess existing structures for the purpose of rehabilitation to achieve a desirable seismic performance following the performance based seismic design philosophy. This inelastic analysis-driven design process requires the evaluation of global load-deformation response of the structures under moderate to high seismic hazard to determine various damage states, which in turn are controlled by the failure modes of the individual components of the structures. This failure mode depends on the material, structural detailing, geometry and multi-axial stress state present in the system. Traditionally axial-flexure interaction has been studied extensively because of its determinate nature of stress condition, while the shear deformation brings an internal indeterminacy which

requires the extra compatibility conditions to reach a unique solution, making the research problem more complex for frame elements.

Continuum finite element analysis is best suited for the simulation of multi-axial stress states present in the system as the degrees of freedom of continuum elements can capture the nonlinear variation of deformations along all the three directions of the geometry simultaneously. However, it needs large numbers of degrees of freedom to reach the converged deformation, which makes it very expensive for analysing global structures.

This research work develops new two-dimensional beam-column frame elements considering axial-flexure-shear interaction through implementing multi-axial constitutive material models for reinforced concrete and steel. Performance evaluation of the developed inelastic frame element formulation with respect to accuracy, efficiency and robustness is essential to satisfy two conditions together: 1. Equilibrium of force in the interior of the element and 2. Displacement compatibility with adjacent elements. Accuracy is a measure of the degree of agreement between the numerical and experimentally-measured response of structural members. Robustness refers to its numerical stability while efficiency refers to the computational cost of the whole member simulation. The element developed adopts a mixed-based formulation that exhibits more robust and accurate behaviour than that of the displacement-based formulation, and is quite efficient for inelastic analysis of large structural systems throughout the loading history.

BACKGROUND

There are several types of steel-concrete composite systems available in the literature. The current research work focuses on conventional two-layer steel-concrete composite deck systems where the concrete slab is connected to the steel beam through shear studs. It was earlier thought that the concrete slab in two-layer composite systems contributes a small amount to the overall shear resistance, and hence concrete contribution in shear has not been included in design standards. However, recent experimental studies (Nie et al., 2004) has proved that the concrete layer provides 33% to 56% shear resistance, which cannot be neglected and should be included into design standards in a rational way. In this type of composite systems, shear studs deform due to their finite stiffness and thus transfer the shear force between the concrete and steel layers. Hence, it is imperative that analysis tool should be capable of simulating the experimentally-observed material inelasticity.

There are mainly two types of analysis procedures used in previous research works, i.e. analytical formulations (Challamel and Girhammar, 2011; and Martinelli et al. 2012) and finite element analysis. The analytical formulations are based on linear elastic material and simple boundary conditions. Therefore, it is difficult to simulate the experimentally-observed behaviour through analytical formulations especially when the complex nature of load resisting process with material nonlinearity under multi-axial stress interactions is involved. On the other hand, finite element analysis can handle this type of behaviour efficiently. There are two types of elements that are generally used in finite element analysis i.e. continuum elements and structural frame elements. Researchers have performed detailed finite element analysis with continuum elements by using available commercial software to reproduce the experimentally-observed responses (Liang et al., 2005; Vasdravellis and Uy, 2014; Liu et al., 2016). However, this type of analysis involves a large number of degrees of freedom and hence, they are suitable for simulation of local regions and often used to calibrate and/or validate frame element models. On the other hand, frame finite element analysis is the alternative one which has been used by various researchers as it can efficiently simulate both local and global behaviour of complete composite structures with reasonable accuracy and much less computational cost compared to that of continuum elements.

Extensive amount of frame finite element studies have been carried out considering axial-flexure interaction in the past. Interested readers are referred to Spacone and El-Tawil, (2004) and Lee and Filippou, (2015) for flexure-critical frame element formulations. The current research work focuses on the simulation of shear-critical composite structures. Schnabl et al. (2007) developed a strain-based Timoshenko composite beam element with partial interaction through the modified principle of virtual work where the strain field vector is the unknown quantity. Silva and Sousa, (2009) presented a displacement-based Timoshenko composite beam element where partial interaction is simulated by zero thickness four-node continuum interface elements. Hjiaj et al. (2012) proposed a displacement-based Timoshenko composite beam element considering nonlinear geometry effect where displacement shape functions are derived from the closed-form solution of the governing differential equations. Chakrabarti et al. (2012) formulated a displacement-based composite beam element considering both longitudinal and vertical slip following higher order beam theory. Batista and Sousa, (2013) proposed a Timoshenko composite beam element with partial interaction for multi-layered systems where the stiffness matrix has been determined by inverting the flexibility matrix which is analytically determined by solving the governing differential equations. Santos and Silberschmidt, (2014) developed an equilibrium-based Timoshenko composite element with

partial interaction where the Lagrangian multiplier method is used to impose inter-element equilibrium. Taig et al. (2015) formulated a composite beam element by considering generalized beam theory where section warping and distortion are built into the formulation. Keo et al. (2016) proposed a displacement-based composite Timoshenko beam element where the prime variables are the slips and shear deformations. So far, all the mentioned element formulations are able to capture the axial-flexure-shear interaction for linear elastic materials only. Zona and Ranzi, (2011) developed a displacement-based Timoshenko fibre composite beam element considering partial interaction where normal and shear stress is uncoupled in the concrete material model. Nguyen et al. (2014) developed a force-based Timoshenko beam element considering both material and nonlinear geometry effect; however, inelastic flexure-shear interaction in concrete is uncoupled. Uddin et al. (2018) developed a displacement-based composite beam element considering higher order beam theory for both material and geometric nonlinearity where axial-flexure-shear interaction is achieved through von Mises plasticity theory with an isotropic hardening rule for concrete in compression and steel; while for concrete in tension, a damage mechanics theory is adopted.

From the above literature survey of frame element formulations of steel-concrete composite members, it can be observed that most of the research works have been performed for linear elastic material considering axial-flexure-shear interaction. Very limited amount of research works have been recently conducted to include inelastic axial-flexure-shear interaction into the frame element formulation with plasticity-based concrete models. Many opportunities remain to implement more efficient and robust reinforced concrete constitutive models developed from shear panel testing to model multi-axial stress states to simulate the softening effect along with cracked Poisson ratio of concrete due to crack-induced anisotropy. So far there are basically two types of fibre element formulations that have been developed which are able to simulate the axial-flexure-shear interaction, i.e. displacement-based and force-based elements. Therefore, there is still a large scope remaining for other types of elements, such as mixed formulations which are more efficient and robust. The current research work aims to extend the two-field mixed-based formulation by Ayoub and Filippou, (2000) to account for shear-critical composite members by implementing coupled multi-axial constitutive laws for materials, along with new stability criteria.

COMPOSITE SHEAR ELEMENT FORMULATION

In this research work, a new shear-critical composite frame element based on distributed inelasticity approach, and considering the partial interaction between the two mediums i.e. steel and concrete, is developed following the Hellinger-Reissner variational principle. Unlike other formulations available in the literature, this element is comprehensive in the sense of constitutive model of materials considering multi-axial coupling among various stress measures and shear deformation in both mediums. Distributed inelasticity-based frame element formulation is essential to develop the inelastic analysis-driven design process such as performance based design methodology for steel-concrete composite systems with partial interaction.

ELEMENT KINEMATICS

The axis of the proposed composite frame element is a straight line joined by nodes I and J in the statically determinate basic reference system in which rigid body displacements are removed by choosing the simple support boundary conditions as shown in Figure (1). The frame element is composed of several sections along its axis. Every section is composed of several fibres which are identified by their position from the reference axis and individual cross-section area.

The section displacement vector $\boldsymbol{u}(x)$ collects two axial translations $u_s(x), u_c(x)$ in the X direction, one translation $v(x)$ in the Y direction, and one rotation $\theta_z(x)$ about the Z axis.

$$\boldsymbol{u}(x) = [u_s(x) u_c(x) \theta_z(x) \quad v(x)]^T \tag{1}$$

It is to be noted that in the current research work, the Engesser-Timoshenko uniform shear model (Challamel and Girhammar, 2011) has been adopted. A differential shear model, where independent rotational degrees of freedom are considered in each layer, will be pursued in future research work.

The element nodal displacement vector $\boldsymbol{u_{IJ}}$collectsthe nodal displacements with respect to global axes according to the section displacement vector in Equation (1). In the proposed composite frame element, an additional middle node with axial and rotational degrees of freedom is included, which will be statically condensed out at the element level before the assembly process:

$$\boldsymbol{u_{IJ}} = \left[u_I^s v_I \theta_{zI} u_I^c u_J^s v_J \theta_{zJ}\ u_J^c u_K^s\ u_K^c \theta_{zK}\right]^T \tag{2}$$

The element deformation vector $\boldsymbol{v}$collects the relative translation u at nodes I, J and K in the X direction, rotations θ_z at nodes I and J and middle node K with respect to the basic reference axes as shown in the Figure (2):

$$\boldsymbol{v} = \left[\theta_{zI} u_{bI}^C u_{bJ}^S \theta_{zJ} u_{bJ}^C u_{bK}^S u_{bK}^C \theta_{zK}\right]^T \tag{3}$$

The relation between element nodal deformation $\boldsymbol{v}$anddisplacements $\boldsymbol{u_{IJ}}$can be uniquely determined by the compatibility matrix $\boldsymbol{a_c}$with constant coefficients under linear geometry conditions, where L is the undeformed length of the element:

$$\boldsymbol{v} = \boldsymbol{a_c u_{IJ}} \tag{4}$$

Where,

$$\boldsymbol{a_c} = \begin{bmatrix} 0 & \frac{1}{L} & 1 & 0 & 0 & -\frac{1}{L} & 0 & 0 & 0 & 0 & 0 \\ -1 & 0 & 0 & 1 & 0 & 0 & 0 & 0 & 0 & 0 & 0 \\ -1 & 0 & 0 & 0 & 1 & 0 & 0 & 0 & 0 & 0 & 0 \\ 0 & \frac{1}{L} & 0 & 0 & 0 & -\frac{1}{L} & 1 & 0 & 0 & 0 & 0 \\ -1 & 0 & 0 & 0 & 0 & 0 & 0 & 1 & 0 & 0 & 0 \\ -1 & 0 & 0 & 0 & 0 & 0 & 0 & 0 & 1 & 0 & 0 \\ -1 & 0 & 0 & 0 & 0 & 0 & 0 & 0 & 0 & 1 & 0 \\ 0 & \frac{1}{L} & 0 & 0 & 0 & -\frac{1}{L} & 0 & 0 & 0 & 0 & 1 \end{bmatrix} \tag{5}$$

SECTION KINEMATICS

The material strain displacement vector $\boldsymbol{\varepsilon}(x, y)$can be related with the section displacement vector $\boldsymbol{u}(x)$as follows:

$$\boldsymbol{\varepsilon}(x, y) = \boldsymbol{a}_s(y)\boldsymbol{d}(x) \tag{6}$$

Where the section deformation vector $\boldsymbol{d}(x)$and section compatibility matrix$\boldsymbol{a}_s(y)$ are:

$$\boldsymbol{d}(x) = \left[\frac{\partial u_s(x)}{\partial x}\ \frac{\partial u_c(x)}{\partial x}\ \frac{\partial \theta_z(x)}{\partial x}\quad \left(-\theta_z(x) + \frac{\partial v(x)}{\partial x}\right)\right]^T \tag{7}$$

$$\boldsymbol{a}_s(y) = \begin{bmatrix} 1 & 0 & -\mathrm{y} & 0 \\ 0 & 1 & -\mathrm{y} & 0 \\ 0 & 0 & 0 & 1 \end{bmatrix} \tag{8}$$

EQUILIBRIUM

The differential equilibrium equation of a segment of length dx of a composite element with shear slip, as shown in Figure (3), can be written down as follows:

$$\boldsymbol{L}^T\boldsymbol{D}(x) - \boldsymbol{L}_b^T\tau_x^b = 0 \tag{9}$$

Where

$$\boldsymbol{D}(x) = [N_x^s N_x^c M_x V_x]^T \tag{10}$$

$$\boldsymbol{L}^T = \begin{bmatrix} \frac{\mathrm{d}}{\mathrm{dx}} & 0 & 0 & 0 \\ 0 & \frac{\mathrm{d}}{\mathrm{dx}} & 0 & 0 \\ 0 & 0 & \frac{\mathrm{d}}{\mathrm{dx}} & -1 \\ 0 & 0 & 0 & \frac{\mathrm{d}}{\mathrm{dx}} \end{bmatrix} \tag{11}$$

$$\boldsymbol{L}_b^T = \begin{bmatrix} -1 \\ 1 \\ \mathrm{H} \\ 0 \end{bmatrix} \tag{12}$$

Here $N_x^s, N_x^c, M_x, V_x, \tau_x^b$ are the axial forces in the steel beam, axial force in the concrete beam, bending moment, shear force and interface bond force per unit length respectively; and H is the distance between the centroids of steel and concrete beams.

COMPATIBILITY

The components of the generalized section deformation vector $\boldsymbol{d}(x)$ are the axial strain ε_0^s in steel, the axial strain ε_0^c in concrete, the curvature $\emptyset_z$ about the z axis and the shear deformation γ_y in the y direction respectively:

$$\boldsymbol{L}\boldsymbol{u}(x) - \boldsymbol{d}(x) = 0 \tag{13}$$

Where

$$\boldsymbol{L} = \begin{bmatrix} \frac{\mathrm{d}}{\mathrm{dx}} & 0 & 0 & 0 \\ 0 & \frac{\mathrm{d}}{\mathrm{dx}} & 0 & 0 \\ 0 & 0 & \frac{\mathrm{d}}{\mathrm{dx}} & 0 \\ 0 & 0 & -1 & \frac{\mathrm{d}}{\mathrm{dx}} \end{bmatrix} \tag{14}$$

The interface slip $S(x)$ between the steel beam and the concrete slab is:

$$S(x) = \boldsymbol{L}_b \boldsymbol{u}(x) \tag{15}$$

where $\boldsymbol{L}_b = [-1 \quad 1 \quad \mathrm{H} \quad 0]$ (16)

CONSTITUTIVE LAW

The section constitutive law is as follows:

$$\boldsymbol{D}(x) = f_{sec}(\boldsymbol{d}(x)) \tag{17}$$

Here f_{sec} is a non-linear function that relates the section force and deformation fields. The section is discretized with 2D fibres. Fibre integration is used to determine the section force-deformation relation.

The bond constitutive law is defined as follows:

$$\tau_x^b = f_{bond}(S(x)) \tag{18}$$

Where f_{bond} is a non-linear function that defines the bond stress-interface slip constitutive law. For the bond-slip constitutive relations, the Eligehausen et al. (1983) law has been used.

MATERIAL MODELS

To couple normal and shear stresses at the material fibre level, multi-axial constitutive laws for materials are essential, which in turn help comprise the interaction of axial force, bending moment and shear force at the element section level. This section presents the constitutive models of steel and reinforced concrete materials implemented in the current study. In this research work, the softened membrane model (Hsu and Zhu, 2001) for concrete; and the J2 plasticity model for steel along with a radial return mapping algorithm, have been adopted to simulate the biaxial interaction between normal and shear stress at the material fibre level. In the following, the significant features of both material models, which have been implemented in this mixed composite shear element for the first time, are presented.

REINFORCED CONCRETE

Three coordinate systems are defined as shown in Figure (4) to formulate the softened membrane model. The local coordinate of the fibre element at the basic frame of reference is defined by the first coordinate system (X, Y).The applied principal stresses of reinforced concrete membrane panel, which has an angle θ_1 with respect to X axis, is represented by the second coordinate system (1, 2); while the rebar coordinate system which has angle $\theta_s$with respect to the X axis is defined by the third coordinate system (X_s, Y_s). The formulation has the capability to consider inclined rebars in the concrete deck; however, in the current research work, the rebars are horizontal. In the current formulation, bond-slip between rebars and concrete has not been considered. However, it is to be noted that the current formulation can be extended to multi-layered composite systems straight forwardly to include the bond-slip between concrete and rebars in the concrete deck as can be seen in Figure 6. The stress vectors in 1-2 and X-Y coordinate axes are represented by$\{\sigma_1\sigma_2\tau_{12}\}^Tand\{\sigma_x\sigma_y\tau_{xy}\}^T$. The strain vectors in 1-2 and X-Y coordinate axes are represented by$\left\{\varepsilon_1\varepsilon_2\frac{1}{2}\gamma_{12}\right\}^T$and $\left\{\varepsilon_x\varepsilon_y\frac{1}{2}\gamma_{xy}\right\}^T$respectively. The biaxial strains from the X-Y system are converted to the 1-2 system through the following transformation matrix:

$$\begin{Bmatrix}\varepsilon_1\\ \varepsilon_2\\ \frac{1}{2}\gamma_{12}\end{Bmatrix} = [T(\theta_1)]\begin{Bmatrix}\varepsilon_x\\ \varepsilon_y\\ \frac{1}{2}\gamma_{xy}\end{Bmatrix} \tag{19}$$

The iterative process of determining $\theta_1$is based on strain state, equilibrium of vertical stress and state of stress; and can be found in details in Mullapudi and Ayoub, (2010).

Equivalent uniaxial strains in the 1-2 system are converted from biaxial strains in the 1-2 system by using cracked concrete Poisson ratio μwhich is known as Hsu/Zhu ratio (Zhu and Hsu, 2002):

$$\begin{Bmatrix} \bar{\varepsilon}_1 \\ \bar{\varepsilon}_2 \\ \frac{1}{2}\gamma_{12} \end{Bmatrix} = [\mu] \begin{Bmatrix} \varepsilon_1 \\ \varepsilon_2 \\ \frac{1}{2}\gamma_{12} \end{Bmatrix} \tag{20}$$

Tensile and compressive strength of concrete has been derived from the equivalent uniaxial smeared stress-strain relation of concrete. However, the compressive strength of concrete depends on the material state of stress. For tensile-compressive state, the compressive strength gets softened due to tensile strains acting in the perpendicular direction. Hsu and Zhu, (2001) derived the following softening coefficient ξ in the compression-tension section, which is employed in the present concrete model:

$$\xi = \left(\frac{5.8}{\sqrt{f_c(MPa)}} \leq 0.9\right)\left(\frac{1}{\sqrt{1+400\bar{\varepsilon}_1}}\right)\left(1 - \frac{|\beta|}{24^\circ}\right) \tag{21}$$

Where,

$$\beta = 0.5\tan^{-1}\left(\frac{\gamma_{12}}{\varepsilon_1 - \varepsilon_2}\right) \tag{22}$$

Where $\bar{\varepsilon}_1$ is the equivalent uniaxial lateral tensile strain and β represents the deviation angle which is determined from the difference between the rotating angle θ_r and the applied stress angle θ_1. For compressive-compressive state of stress, the enhanced compressive strength due to the compressive stress acting in the perpendicular direction through the enhancement factor developed by Vecchio, (1992) and Kupfer et al. (1969) has also been considered. However, the tensile strength of concrete gets influenced in a very minimal way due to the presence of perpendicular tensile stresses.

The uniaxial compressive softened monotonic stress-strain relation defined by Hsu and Zhu, (2001) is adopted in this study. The uniaxial tensile stress-strain relation of concrete developed

by Zulfiqar and Filippou, (1990) which can simulate tensile stiffening effect due to rebars, has been used in this research work with the above mentioned softened stress-strain relationship.
Once the strength of concrete has been determined in the equivalent uniaxial 1-2 coordinate system, shear strength and stiffness (G) can be developed as follows (Zhu et al., 2001):

$$G = \frac{\sigma_1 - \sigma_2}{\varepsilon_1 - \varepsilon_2} \tag{23}$$

$$\tau_{12}\ at\ (t+1) = \tau_{12}\ at\ (t) + G(\Delta\frac{\gamma_{12}}{2}) \tag{24}$$

The equivalent uniaxial strain of concrete can be transformed into uniaxial strain of rebars as follows:

$$\begin{Bmatrix} \bar{\varepsilon}_{1s} \\ \bar{\varepsilon}_{2s} \\ \frac{1}{2}\gamma_{12} \end{Bmatrix} = [T(\theta_s - \theta_1)] \begin{Bmatrix} \bar{\varepsilon}_1 \\ \bar{\varepsilon}_2 \\ \frac{1}{2}\gamma_{12} \end{Bmatrix} \tag{25}$$

The stress and stiffness of rebars can be determined from the uniaxial rebar model. In this study, the inelastic model developed by Menegotto and Pinto, (1973) and Filippou et al. (1983) has been adopted for the rebars in the reinforced concrete deck. However, the effect of concrete on rebar needs to be accounted for as proposed by Belarbi and Hsu, (1994).
The stress vector of reinforced concrete panel in the X-Y coordinate system is determined from the following equilibrium equations:

$$\begin{Bmatrix} \sigma_x \\ \sigma_y \\ \tau_{xy} \end{Bmatrix} = [T(-\theta_1)] \begin{Bmatrix} \sigma_1 \\ \sigma_2 \\ \tau_{12} \end{Bmatrix} + \sum_i [T(-\theta_{si})] \begin{Bmatrix} \rho_{si}\sigma_{si} \\ 0 \\ 0 \end{Bmatrix} \tag{26}$$

Here, ρ_{si} is the average steel ratio in direction i.
The 2D fibre stiffness matrix $[D]$ of reinforced concrete material in the X-Y coordinate system can be determined from the equivalent uniaxial stiffness of concrete and steel at their respective coordinate systems as follows:

$$[D] = [D_{concrete}] + [D_{steel}] \tag{27}$$

Where,

$$[D_{concrete}] = [T(-\theta_1)][D_{uniaxial}^{concrete}][\mu][T(\theta_1)] \quad (28)$$

$$[D_{steel}] = \sum_i \quad [T(-\theta_{si})]\left[D_{uniaxial}^{steel\_i}\right][T(\theta_{si} - \theta_1)][\mu][T(\theta_1)] \quad (29)$$

$$[D_{uniaxial}^{concrete}] = \begin{bmatrix} E_{t1} & D_{12} & 0 \\ D_{21} & E_{t2} & 0 \\ 0 & 0 & G \end{bmatrix} \quad (30)$$

Here $D_{12} = \frac{d\sigma_1}{d\bar{\varepsilon}_2}$ and $D_{21} = \frac{d\sigma_2}{d\bar{\varepsilon}_1}$ are coupling material stiffness terms which exist only for a tensile-compressive state of strain due to the presence of the softening coefficient.

$$\left[D_{uniaxial}^{steel\_i}\right] = \begin{bmatrix} \rho_{si}E_t & 0 & 0 \\ 0 & 0 & 0 \\ 0 & 0 & 0 \end{bmatrix} \quad (31)$$

STRUCTURAL STEEL

To simulate the biaxial interaction between normal and shear stresses at the material fibre level for steel beam sections, the J2 plasticity model has been implemented in this study. The significant features of the J2 plasticity model along with the implemented radial return mapping algorithm is presented in the following discussion.

The yield function is defined by the deviatoric stress **s**, the back stress variable $\boldsymbol{s_b}$representing the distance of yield surface centre from the origin of the deviatoric stress space, and the linear isotropic hardening modulus H_i:

$$f(\boldsymbol{s}, \boldsymbol{s_b}, H_i) = \|\boldsymbol{s} - \boldsymbol{s_b}\| - \sqrt{\frac{2}{3}}(\sigma_y + H_i\beta) \quad (32)$$

Here, σ_y is the uniaxial tensile yield strength and β is the isotropic hardening variable with nature of plastic strain.

The plastic flow rule is:

$$\dot{\boldsymbol{e_p}} = \alpha\frac{\partial f}{\partial \boldsymbol{s}} \quad (33)$$

Here α and $\frac{\partial f}{\partial \boldsymbol{s}}$are the plastic consistency parameter and the normal to the yield surface respectively:

$$\frac{\partial f}{\partial \boldsymbol{s}} = \frac{(\boldsymbol{s}-\boldsymbol{s_b})}{\|\boldsymbol{s}-\boldsymbol{s_b}\|} \tag{34}$$

The hardening rules are:

$$\dot{\beta} = \sqrt{\frac{2}{3}}\alpha \tag{35}$$

$$\dot{\boldsymbol{s_b}} = \frac{2}{3}\dot{\alpha}H_k\frac{\partial f}{\partial \boldsymbol{s}} \tag{36}$$

Where H_k is the kinematic hardening modulus.
The plastic consistency parameter α satisfies the following loading and unloading Kuhn-Tucker conditions:

$$\dot{\alpha} \geq 0, \quad f \leq 0, \quad \dot{\alpha}f = 0 \tag{37}$$

Also, the following consistency condition needs to be satisfied:

$$\alpha\dot{f} = 0 \tag{38}$$

A step by step summary of the material state determination through the integration of the above mentioned governing equations with the backword-Euler integration scheme, which results in a radial return mapping algorithm, is presented in Figure (5) for a single material point. A more detailed explanation can be found in Saritas and Filippou, (2009) and Simo and Hughes, (1998). The summary focuses on a single iteration i for reaching vertical stress equilibrium at the material point (Klinkel and Govindjee, 2002).

DISPLACEMENT-BASED FORMULATION

The principle of virtual displacements forms the basis of the principle of minimum potential energy that uses displacements as the only independent field. The potential energy functional

($\prod_p$) is written in terms of the independent nodal displacement (u) field in the basic frame of reference which does not include rigid body motions as follows:

$$\prod_p(u) = \int_v W(\varepsilon^u(x,y))\,dv + \prod_b(u(x)) - \prod_{ext}(u(x)) - \prod_{bc}(u) \quad (39)$$

The potential energy functional of Equation (39) can be written without body force and surface traction with section level variables in the following form:

$$\prod_p(u) = \int_L d^T(x)\,D(x)\,dx + \int_L s^T(x)\,\tau_x^b(x)\,dx - u^T P^* \quad (40)$$

where P^* is the applied nodal boundary forces.

Transformation of this functional from the material level to the section level needs a compatibility condition through appropriate section kinematics. In this formulation, distributed inelasticity at the section level is considered through fibre discretization. The section resisting force and stiffness are obtained from the integration of the fibre level variables. It is to be noted that by adopting a fibre model, coupling of axial, shear and bending response is a natural process. This is a significant advantage over section-based models where coupling needs extra care through plasticity formulations.

The variation of potential energy functional in Equation (40) can be written in the following form:

$$\delta\prod_p(\boldsymbol{u}) = \int_L \delta\boldsymbol{d}^T(x)\,\boldsymbol{D}(x)\,dx + \int_L \delta s^T(x)\,\tau_x^b(x)\,dx - \delta\boldsymbol{u}^T\boldsymbol{P}^* \quad (41)$$

The solution of the variational in Equation (41) is non-linear under inelastic material conditions, so the problem is linearized about a state $\boldsymbol{u}^i$ as follows:

$$\delta\prod_p(\boldsymbol{u^{i+1}}) = \delta\prod_p(\boldsymbol{u^i}) + \frac{\partial\delta\prod_p(\boldsymbol{u})}{\partial u}\Big|_{\boldsymbol{u}^i}\Delta\boldsymbol{u} \quad (42)$$

Where $\Delta\boldsymbol{u}$ is the incremental nodal displacement vector.

At equilibrium, Equation (42) can be written in the following expanded form:

$$\int_L \delta \boldsymbol{d}^T(x)\, \boldsymbol{D^i}(x)\, dx + \int_L \delta \boldsymbol{s}^T(x)\, \tau_x^{b,i}(x)\, dx - \delta \boldsymbol{u}^T \boldsymbol{P}^* + \left(\int_L \delta \boldsymbol{d}^T(x) \frac{\partial \boldsymbol{D}(x)}{\partial \boldsymbol{u}}\, dx + \int_L \delta \boldsymbol{s}^T(x) \frac{\partial \tau_x^b}{\partial \boldsymbol{u}}\, dx - \delta \boldsymbol{u}^T \frac{\partial P^*}{\partial u}\right) \Delta \boldsymbol{u} = 0 \quad (43)$$

By using Equations (9), (13), (15), (17) and (18) and assuming conservative applied loads, and from arbitrariness of $\delta \boldsymbol{u}$, Equation (43) can be written in the following expanded form:

$$\left(\int_L \boldsymbol{B_s}^T(x)\, \boldsymbol{K_s}(x) \boldsymbol{B_s}(x) dx + \int_L \boldsymbol{B_b}^T(x) \boldsymbol{K_b}(x) \boldsymbol{B_b}(x)\, dx\right) \Delta \boldsymbol{u} = \boldsymbol{P}^* - \int_L \boldsymbol{B_s}^T(x)\, \boldsymbol{D^i}(x)\, dx - \int_L \boldsymbol{B_b}^T(x)\, \tau_x^{b,i}(x)\, dx \quad (44)$$

Where, $\boldsymbol{B_s}(x)$ and $\boldsymbol{B_b}(x)$ are the strain-displacement and slip-displacement matrices.

Equation (44) can be written in the following concise form:

$$(\boldsymbol{K_{c+s}} + \boldsymbol{K_B}) \Delta \boldsymbol{u} = \boldsymbol{P}^* - \boldsymbol{P^r_{c+s}} - \boldsymbol{P^r_b} \quad (45)$$

$$\boldsymbol{K} \Delta \boldsymbol{u} = \boldsymbol{P}^* - \boldsymbol{P^r} \quad (46)$$

where $\boldsymbol{K}$ is the composite element stiffness matrix which consists of the combined concrete and steel beam stiffness $\boldsymbol{K_{c+s}}$ and bond stiffness $\boldsymbol{K_B}$, and $\boldsymbol{P^r}$ is the composite element resisting vector which consists of the combined concrete and steel beam resisting forces $\boldsymbol{P^r_{c+s}}$ and the bond resisting force $\boldsymbol{P^r_b}$. The detailed state determination process of the displacement-based formulation can be found in Das (2019).

MIXED-BASED FORMULATION

The composite beam element with partial interaction has been formulated by using independent fibre displacements and stress functions following the two-field Hellinger-Reissner (HR) functional which is written in the basic frame of reference as follows:

$$\prod_{HR}(\boldsymbol{u}, \boldsymbol{\sigma}) = -\int_v W\left(\boldsymbol{\sigma}(x,y)\right) dv + \int_v \boldsymbol{\sigma}^T \boldsymbol{\varepsilon^u}\, dv + \prod_b(\boldsymbol{u}(x)) - \prod_{ext}\left(\boldsymbol{u}(x)\right) - \prod_{bc}(\boldsymbol{u}) \quad (47)$$

Where $W(\boldsymbol{\sigma})$ is the complementary energy function.

HR energy functional of Equation (47) can be written without body forces and surface tractions with section level variables in the following form:

$$\prod_{HR}(\boldsymbol{u},\boldsymbol{p}) = -\int_0^L \boldsymbol{D}^T\boldsymbol{d}(\boldsymbol{D})\,dx + \int_0^L \widehat{\boldsymbol{D}}^T(\boldsymbol{p})\boldsymbol{d}(\boldsymbol{u})\,dx + \int_0^L \boldsymbol{s}^T(\boldsymbol{u})\,\tau_x^b\,dx - \boldsymbol{u}^T\boldsymbol{P}^* \tag{48}$$

In this element formulation, the beam section forces $\widehat{\boldsymbol{D}}$ are independently derived from the element nodal forces $\boldsymbol{p}$degree of freedom as follows:

$$\widehat{\boldsymbol{D}}(x) = \boldsymbol{b}(x)\,\boldsymbol{p} \tag{49}$$

$$\boldsymbol{b}(x) = \begin{bmatrix} 1-\frac{x}{L} & \frac{x}{L} & 0 & 0 & 0 & 0 \\ 0 & 0 & 1-\frac{x}{L} & \frac{x}{L} & 0 & 0 \\ 0 & 0 & 0 & 0 & \frac{x}{L}-1 & \frac{x}{L} \\ 0 & 0 & 0 & 0 & -\frac{1}{L} & -\frac{1}{L} \end{bmatrix} \tag{50}$$

Here $\boldsymbol{b}(x)$ is the matrix of force interpolation functions which has been derived by coalescing the centroids of both layers through a single reference point.

It is to be noted that bond forces are determined through bond constitutive relations. Therefore, the equilibrium matrix $\boldsymbol{b}(x)$ only satisfies the differential equilibrium Equation (9) partially without the contribution of bond stresses. It is in synchronization with HR energy functional as in this variational principle there is no subsidiary condition required. However, the composite element formulation derived from the complementary energy functional loses its most powerful credibility for not satisfying the differential equilibrium equations in their strong form fully.

The variation of HR energy functional in Equation (48) can be written in the following form:

$$\delta\prod_{HR}(\boldsymbol{u},\boldsymbol{p}) = -\int_0^L \delta\boldsymbol{D}^T\boldsymbol{d}(\boldsymbol{D})\,dx + \int_0^L \delta(\widehat{\boldsymbol{D}}^T(\boldsymbol{p}))\boldsymbol{d}(\boldsymbol{u})\,dx + \int_0^L (\widehat{\boldsymbol{D}}^T(\boldsymbol{p}))\delta(\boldsymbol{d}(\boldsymbol{u}))\,dx + \int_0^L \delta\boldsymbol{s}^T(x)\,\tau_x^b(x)\,dx - \delta\boldsymbol{u}^T\boldsymbol{P}^* \tag{51}$$

Under inelastic material state, the solution of the variational in Equation (51) becomes non-linear, hence the nonlinear function needs to be linearized with respect to a state of both principle arguments$\boldsymbol{u}^i$ and $\boldsymbol{p}^i$ as follows:

$$\delta \prod_{HR}(\boldsymbol{p^{i+1}}, \boldsymbol{u^{i+1}}) = \delta \prod_{HR}(\boldsymbol{p^i}, \boldsymbol{u^i}) + \frac{\partial \delta \prod_{HR}(\boldsymbol{p},\boldsymbol{u})}{\partial p}|_{\boldsymbol{p^i},\boldsymbol{u^i}} \Delta \boldsymbol{p} + \frac{\partial \delta \prod_{HR}(\boldsymbol{p},\boldsymbol{u})}{\partial u}|_{\boldsymbol{p^i},\boldsymbol{u^i}} \Delta \boldsymbol{u} \quad (52)$$

Where $\Delta \boldsymbol{p}$ and$\Delta \boldsymbol{u}$are the incremental nodal force and displacement vector respectively.
At equilibrium, from Equation (52), the following equation can be written:

$$\delta \prod_{HR}(\boldsymbol{p^i}, \boldsymbol{u^i}) + \frac{\partial \delta \prod_{HR}(\boldsymbol{p},\boldsymbol{u})}{\partial p}|_{\boldsymbol{p^i},\boldsymbol{u^i}} \Delta \boldsymbol{p} + \frac{\partial \delta \prod_{HR}(\boldsymbol{p},\boldsymbol{u})}{\partial u}|_{\boldsymbol{p^i},\boldsymbol{u^i}} \Delta \boldsymbol{u} = 0 \quad (53)$$

By using Equations (9), (13), (15), (17), (18) and (49) along with the assumption of conservative external load, Equation (53) can be written in the following form:

$$\delta \boldsymbol{u}^T \left[\int_0^L \boldsymbol{B}_s^T(x)\, \boldsymbol{b}(x)\, dx\, \Delta \boldsymbol{p} + \int_0^L \boldsymbol{B}_b^T(x)\, \boldsymbol{K_b}(x) \boldsymbol{B}_b(x) dx\, \Delta \boldsymbol{u} + \int_{\boldsymbol{0}}^{\boldsymbol{L}} \boldsymbol{B}_{\boldsymbol{s}}^T \boldsymbol{D}(x) dx + \int_{\boldsymbol{0}}^{\boldsymbol{L}} \boldsymbol{B}_{\boldsymbol{b}}^T \tau_x^b(x) dx - \boldsymbol{P}^* \right] + \delta \boldsymbol{p}^T \left[- \int_0^L \boldsymbol{b}^T(x) \boldsymbol{f_s}(x) \boldsymbol{b}(x) dx \Delta \boldsymbol{p} + \int_0^L \boldsymbol{b}^T(x) \boldsymbol{B_s}(x) dx \Delta \boldsymbol{u} + \int_0^L \boldsymbol{b}^T(x)\, \boldsymbol{d}(x) dx - \int_0^L \boldsymbol{b}^T(x)\, \widehat{\boldsymbol{d}}(x) dx \right] = 0 \quad (54)$$

where $\boldsymbol{f_s}(x)$ is the section flexibility matrix and $\widehat{\boldsymbol{d}}(x)$ is the section deformation vector determined from section force vector $\widehat{\boldsymbol{D}}(x)$ with the help of the section flexibility matrix.
From arbitrariness of $\delta \boldsymbol{u}$and $\delta \boldsymbol{p}$, Equation (54) can be written in the following matrix form:

$$\begin{bmatrix} \int_0^L \boldsymbol{B}_b^T \boldsymbol{K}_b \boldsymbol{B}_b dx & \int_0^L \boldsymbol{B}_s^T \boldsymbol{b} dx \\ \int_0^L \boldsymbol{b}^T \boldsymbol{B}_s\, dx & -\int_0^L \boldsymbol{b}^T \boldsymbol{f}_s \boldsymbol{b} dx \end{bmatrix} \begin{pmatrix} \Delta \boldsymbol{u} \\ \Delta \boldsymbol{p} \end{pmatrix} = \begin{pmatrix} \boldsymbol{P}^* - \int_0^L \boldsymbol{B}_s^T \boldsymbol{D} dx - \int_0^L \boldsymbol{B}_b^T \tau_x^b dx \\ \int_0^L \boldsymbol{b}^T (\widehat{\boldsymbol{d}} - \boldsymbol{d}) dx \end{pmatrix} \quad (55)$$

Equation (55) can be written in the following concise form:

$$\begin{bmatrix} \boldsymbol{K}_B & \boldsymbol{G}^T \\ \boldsymbol{G} & -\boldsymbol{F}_{\boldsymbol{c+s}} \end{bmatrix} \begin{pmatrix} \Delta \boldsymbol{u} \\ \Delta \boldsymbol{p} \end{pmatrix} = \begin{pmatrix} \boldsymbol{P}^* - \boldsymbol{P}_{\boldsymbol{c+s}}^{\boldsymbol{r}} - \boldsymbol{P}_{\boldsymbol{b}}^{\boldsymbol{r}} \\ \boldsymbol{u}^r \end{pmatrix} \quad (56)$$

Here, $\boldsymbol{F}_{c+s}$ is the element flexibility matrix, $\boldsymbol{G} = \int_0^L \boldsymbol{b}^T \boldsymbol{B}_s\, dx$, and $\boldsymbol{u}^r$ is the element residual deformation vector. To satisfy element level compatibility, the element residual deformation vector $\boldsymbol{u}^r$needs to be iterated until convergence to make it virtually zero.
Two different numerical algorithms are possible for the two-field mixed element formulation. In the first algorithm, both element independent nodal displacement and force degrees of

freedom become available to the solver and the solution of Equations (56) are carried out by the solver simultaneously for both fields. However, with this algorithm the force fields become continuous between inter-element boundaries, which may not represent the actual scenarios under concentrated loading conditions. The implementation of this first strategy is rare in finite element analysis as a global solver needs to be coded for both displacement and force variables, and therefore, this algorithm has not been adopted in this research work.

The second algorithm considers the static condensation of the element nodal force field from Equation (56) and makes available only the element nodal displacement degrees of freedom to the solver, which is very common in finite element analysis. As a result, the force field is not continuous at element boundaries.

In a nonlinear structural analysis algorithm, the element state determination defines the computations of the element resisting force vector and the element tangent stiffness matrix corresponding to the given current element nodal displacements and their increments.

In this formulation, after the static condensation of the force fields at the element level, Equation (56) becomes:

$$\boldsymbol{G}^T[\boldsymbol{F}_{c+s}^{-1}][\boldsymbol{G}\Delta\boldsymbol{u} - \boldsymbol{u}^r] + \boldsymbol{K}_B\Delta\boldsymbol{u} = \boldsymbol{P}^* - \boldsymbol{G}^T\boldsymbol{P}_{c+s}^r - \boldsymbol{P}_b^r \tag{57}$$

Here, the choice of storing of element residual deformation vector $\boldsymbol{u}^r$ in Equation (57) between subsequent global iterations creates two algorithms. A non-iterative solution algorithm where no internal element iteration is necessary exists, as storing element residual deformations is eliminated through the inclusion of $\boldsymbol{u}^r$ in the element forces at the basic frame of reference. Whereas for an iterative solution algorithm, internal element iterations are necessary until the deformation vector is adjusted to satisfy compatibility at the element level by forcing the element residual deformation vector $\boldsymbol{u}^r$ to reach a value less than a tolerance amount.

In this formulation, an iterative solution algorithm has been adopted and the choice of displacement and force interpolation functions follows the Babuska-Brezzi condition along with the principle of limitation (De Veubeke, 1965). However, it has been established by Ayoub, (2001) that the principle of limitation criteria is the prime governing criteria to choose the correct order of displacement and force interpolation functions to achieve an accurate solution. Stability criteria of the mixed formulation are described in the following section. Once convergence is reached at the element level, i.e. $\boldsymbol{u}^r$ becomes zero, Equation (57) can be written as follow:

$$(\boldsymbol{G}^T[\boldsymbol{F}_{c+s}^{-1}]\boldsymbol{G} + \boldsymbol{K}_B)\Delta\boldsymbol{u} = \boldsymbol{P}^* - \boldsymbol{G}^T\boldsymbol{P}_{\boldsymbol{c+s}}^{\boldsymbol{r}} - \boldsymbol{P}_{\boldsymbol{b}}^{\boldsymbol{r}} \quad (58)$$

$$(\boldsymbol{K}_{\boldsymbol{c+s}} + \boldsymbol{K}_{\boldsymbol{B}})\Delta\boldsymbol{u} = \boldsymbol{P}^* - \boldsymbol{G}^T\boldsymbol{P}_{\boldsymbol{c+s}}^{\boldsymbol{r}} - \boldsymbol{P}_{\boldsymbol{b}}^{\boldsymbol{r}} \quad (59)$$

$$\boldsymbol{K}\Delta\boldsymbol{u} = \boldsymbol{P}^* - \boldsymbol{P}^{\boldsymbol{r}} \quad (60)$$

A step by step summary of the state determination algorithm is presented in Table (1) for a single composite element. The summary focuses on a single global iteration i at the structural level through the Newton-Raphson method with a load counter k. The nodal displacements of the structural model in the global frame of reference are collected in the displacement vector$\boldsymbol{U}^g$. The detailed procedure of mapping structural nodal displacements relative to global coordinates to the element nodal deformations at the basic frame of reference, transformation of element stiffness matrix and resisting forces from basic to global level, and assembling of global stiffness matrix and resistance forces of all elements to the assembled structural stiffness matrix $\boldsymbol{K}^g$ and structural resistance vector $\boldsymbol{P}^{gr}$are described in details in Filippou and Fenves, (2004).

STABILITY CRITERIA – MIXED FORMULATION

The order of displacement (n_d) and force (n_f) shape functions are interconnected through the compatibility and constitutive relations in the two-field mixed-based formulation. The order and continuity of both shape functions are critical in mixed-based formulations; otherwise non-meaningful results will be produced as observed by Zienkiewicz and Taylor, (1989). Stability of the algorithm can be achieved by following De Veubeke's principle of limitation (1965) which states that the order of stress field should be less or equal than that of strain field.

For flexure-critical mixed composite element formulations (Ayoub and Filippou, 1999), a linear axial force distribution without the presence of axially distributed loads, requires quadratic distribution of axial displacements along the length of the element. Whereas, a linear moment field requires a linear curvature field which in turn requires cubic distribution of the vertical displacement field along the axial direction of the element. Using Hermitian polynomial shape functions for the vertical displacement field, two-node beam elements will be sufficient for the dependent rotation field to satisfy the principle of limitation stability criteria for flexure-critical conditions. However, one additional middle degree of freedom for

the axial field needs to be included, which will get statically condensed out at the element level before the assembly process.

For shear-critical mixed composite element formulations, a linear axial force distribution without the presence of axially distributed loads, requires quadratic distribution of axial displacements. Whereas, a linear moment field requires a linear curvature field which in turn requires a quadratic distribution of the rotation field along the length of the element. As for shear, a constant shear force distribution along the length of the element requires a cubic vertical displacement field to match the same order of the rotation field. Therefore, the following relations are proposed for the newly developed shear-critical mixed element:

For the axial field:

$$n_f = n_d - 1 \tag{61}$$

For the moment field:

$$n_f = n_d - 1 \tag{62}$$

For the shear field:

$$n_f = n_d - 3 \tag{63}$$

Using quadratic polynomial shape functions for axial and rotational fields, two-node beam elements will not be sufficient to satisfy the principle of limitation stability criteria for shear-critical conditions. Therefore, one additional middle degree of freedom for the axial and rotation field is a must for shear-critical two-field mixed beam elements, which will get statically condensed out at the element level before the assembly process.

CORRELATION STUDIES

This section presents several correlation studies of the newly developed composite beam element with partial interaction based on two-field mixed formulations for shear critical steel-concrete composite members. Two different types of composite systems are considered for the correlation studies, i.e. steel-concrete-steel sandwiched systems and conventional steel-

concrete composite deck systems; to establish the versatility of the proposed composite beam element. Larger energy dissipation capacity of steel-concrete sandwiched components compared to that of reinforced concrete members, make it more cost effective and efficient for seismic and blast-resistance systems. The correlation studies start with a numerical evaluation of sandwiched steel-concrete composite beams followed by a steel-concrete composite deck system to validate the newly developed composite element formulation with the implemented multi-axial material models.

STEEL-CONCRETE-STEEL COMPOSITE BEAM

A sample sandwiched beam problem (Figure 6) is analysed to determine the efficiency and accuracy of the newly developed mixed-based composite element formulation by comparing the responses derived from the displacement-based formulation. The beam span is 2000 mm and is under a central point vertical loading with simply supported boundary conditions. The shear span to depth ratio is 3.3. The top and bottom plate thickness is 8 mm each. The concrete section depth is 288 mm. The width of the beam section is 300 mm. The diameter of tie bars is 9.5 mm and the spacing is 240 mm along the length of the beam and 200 mm along the section width. The headed studs' diameter is 13 mm and the spacing is 120 mm along the length of the beam and 100 mm along the section width. The concrete compressive strength is 26.8 MPa. The yield strength of steel is 350 MPa and bond strength of shear studs is 317 MPa.

It is to be noted that to model sandwiched members, the degrees of freedom at the section and element level need to be adjusted accordingly. Two, eight, and twenty elements have been used to model the entire beam specimen for the displacement-based formulation; while only two elements are used for the mixed-based formulation along with 5 section integration points in each element for both formulations.

Figure (7) presents the comparison of vertical load versus mid-point deflection response between the mixed-based and displacement-based formulations. It can be observed that the displacement-based formulation needs 20 elements to accurately simulate the inelastic global load-deflection response compared to that of mixed-based formulation with 2 elements. The bending moment distributions at different load stages, for both the displacement and mixed models are shown in Figures (8) and (9) respectively. The two load stages A and B are shown in Figure (7).

In the absence of any distributed loads, the bending moment distribution is linear which does not depend on the existence of bond shear forces at the interface levels. The mixed model is able to predict the exact linear moment distribution as shown in Figure (9), while the

displacement model fails to do so with a small number of elements as shown in Figure (8), and converges to the true distribution only when a large number of elements were used.

Figures (10) and (11) show the top plate axial force distributions for both models. The mixed model clearly better predicts the axial force distribution than that of the displacement-based model, which also reveals nonlinearity and jumps at inter-element boundaries.

Figures (12) and (13) depict the shear force distributions at different load stages for both the displacement and mixed models respectively. The displacement-based formulation needs more elements to accurately simulate the shear force distribution, although slight jumps are observed at the element boundaries. The mixed-based formulation accurately reproduces a constant shear force distribution with only 2 elements.

Figures (14) and (15) show the bottom interface slip distributions for both models. The displacement-based formulation does not produce any jumps at element boundaries as the slip field is directly determined from the element nodal deformations. However, it needs larger number of elements to reasonably reproduce the comparable slip distribution with that of the mixed-based formulation.

This numerical example has established that the newly developed mixed element formulation is more accurate, efficient and computationally less expensive than the element formulation based on the displacement approach.

COMPOSITE BEAM of NIE et al. (2004)

Nie et al. (2004) carried out static monotonic tests on a series of 16 steel-concrete composite beams to investigate the effect of shear span aspect ratio, as well as the width and thickness of the concrete flanges on the shear resisting mechanisms and strength of composite beams. It has been concluded that the concrete shear contribution by the concrete flange is 33% to 56% of the applied total ultimate shear, which motivated the development of the composite beam element with partial interaction considering inelastic axial-flexure-shear interaction in both concrete and steel materials. Two types of shear failure modes in the concrete flange have been observed in the experiment, i.e. diagonal tension failure and diagonal shear crushing. Shear yielding followed by local buckling in the web of steel sections has also been observed in the experiment for those specimens which failed in a shear mode.Out of these specimens, the composite beam CBS-2, in which a shear failure mode has been observed in the experiment, is chosen for the purpose of the correlation study. The beam span is 2800 mm. The beam is under two-point vertical loading 600 mm away from each end. The shear span to depth ratio is 2.0. The cross-section details of the composite beam are shown in Figure (16). The width and depth

of the concrete flange is 680 mm and 100 mm respectively. Reinforcement in the concrete flange along the beam axial direction and across the section width is provided with 100 mm spacing and a diameter of 6 mm. The diameter of headed studs is 8 mm, and they are spaced 90 mm along the length of the beam and 80 mm along the section width. The concrete compressive strength is 30.06 MPa. The yield strength of steel in the web and flange regions is 340 MPa and 273 MPa respectively. The bond strength of shear stud is considered to be 346 MPa.

Four elements have been used to model the entire composite beam specimen using the mixed-based formulation with 5 section integration points in each element. Figure (17) presents the vertical load versus mid deflection response of the member; and it can be observed that the newly developed mixed-based composite beam element with partial interaction has reasonably reproduced the overall experimentally-observed load-deflection response. The shear stiffness, ultimate shear resistance, and shear deformation capacity have been captured well by the model. It is also noted that the shear resistance capacity gets increased while the shear deformation capacity gets decreased when full interaction is considered by increasing the bond stiffness of shear studs. An opposite behaviour can also be observed when the bond stiffness is reduced significantly for the no-interaction situation. These observations emphasize the necessity to the formulation of shear critical composite frame elements with partial interaction to simulate the shear behaviour accurately, which in turn will help to develop an inelastic analysis-driven design process of composite members. It can also be observed that 4, 14 and 28 elements using the displacement-based formulation and 4 elements using the mixed-based formulation produce essentially the same global load-deflection response under four point loading conditions.

Figures (18) and (19) show the shear force and bending moment distributions respectively along the length of the beam in the inelastic zone of the load-deflection response, i.e. point A in Figure (17). It can be observed that both displacement and mixed formulations have excellently produced a smooth variation of shear force along the length of the beam. Similar observation of shear force distribution has also been reported by Zona and Ranzi, (2011) with displacement-based elements. However, jumps about the true distribution of bending moment obtained at element boundaries have been observed for the displacement-based formulation.

Figure (20) shows the interface slip distribution along the length of the beam in the inelastic zone of load-deflection response, i.e. point A in Figure (17). It can be observed that both displacement and mixed formulations have essentially produced almost the same distribution

of relative slip along the length of the beam, as the slip field has been determined from nodal displacement degrees of freedom for both formulations.

The axial force distributions at point A in Figure (17) for the steel and concrete sections are shown in Figures (21) and (22) respectively. It can be observed that the mixed formulation with 4 elements has excellently produced a smooth linear variation of axial force along with exact equilibrium between steel and concrete axial section forces. However, the displacement-based formulation has shown a jump at element boundaries, and reasonable performance has been achieved only when the number of elements has increased to 28. It is to be noted that larger number of elements are required to successfully simulate the local response using displacement-based formulations compared to that of the global response.

Figure (23) shows the distribution of the applied stress angle θ_1 (Figure 4) along the length of the beam at point A in Figure (17) for the middle fibre of the concrete section. It can be observed that the mixed formulation has excellently produced the accurate variation of applied stress angle as observed in the experiment. Meanwhile, the displacement formulation has shown a reasonable performance only when the number of elements has been greatly increased.

Figure (24) shows the curvature-loading response at the loading point. It can be observed that the mixed formulation with 4 elements excellently produced localized curvature distributions compared to that of the displacement based formulation with 28 elements.

From Figure (25), it can be observed that the principle compressive strain of the top concrete fibre in the concrete deck reached a substantial amount. The displacement-based formulation was not able to produce a good result, even with 28 elements.

Figure (26) shows the axial strain-loading response of the bottom rebar in the concrete deck at the loading point. It can be observed that the strain does not exceed the yield limit and it started unloading at the later stage of loading to satisfy equilibrium. This signifies that flexural action does not dominate in the concrete deck. This local behaviour has been excellently produced by the mixed formulation. The displacement-based formulation was not able to reproduce this type of local behaviour even with large number of elements.

Figure (27) shows the axial strain-loading response in the compression rebar at the concrete section. It is to be noted from Figure (22) that the concrete section remains under compressive stress conditions. It should be realized that the compressive strain in the top rebar started unloading at the later stage of loading. As a result, the rebar reaches the tensile zone, and also the peak amount of compressive strain is substantially less than that of the top concrete fibre (Figure 25). This observation indicates that the flexure energy in the concrete deck does not

play an important role at the later stage of loading as the shear energy dominates and resists the external input energy.

The aforementioned results have verified the superiority of mixed-based formulations relative to the displacement-based approach. These results confirm that the proposed mixed formulation is capable of simulating the global and local behaviour of shear critical composite beams along with failure modes. Moreover, the inherent limitation of displacement-based formulation to reproduce local behaviour, even with large number of elements, is a warning sign. The need of mixed-based shear composite elements, which can successfully reproduce local behaviour and help to formulate inelastic analysis-driven design process, has been established through this research work.

CONCLUSION

A new composite beam element formulation is presented following two-field mixed-based variational principles and considering bond-slip and axial-flexure-shear interaction, which are essential to accurately simulate the stiffness, resistance and deformation capacity of shear-critical partially-connected steel-concrete composite members. A robust state determination along with new stability criteria for the mixed-based formulation has been proposed. Softening of compressive strength of concrete under compressive-tensile biaxial state of stress along with cracked Poisson ratio due to crack-induced anisotropy has been considered explicitly in the formulation of beam-column composite element with partial interaction. Numerical studies of experimentally-tested shear-critical composite beams established the accuracy and efficiency of the mixed formulation over the standard displacement-based model with respect to local deformations and force fields, along with considerable reduction of computational cost; which will be very useful in the development of performance-based design procedures for composite structures.

ACKNOWLEDGEMENTS

The first author is grateful to the University Doctoral Studentship awarded by City, University of London, and is very honoured to be the recipient of this prestigious scholarship.

REFERENCES

Ayoub, A. S., and Filippou, F. C. (1999). “Mixed formulation of bond slip problems under cyclic loads.” *J. Struct. Eng*., 125 (6), 661-671.

Ayoub, A., and Filippou, F. C. (2000). “Mixed formulation of nonlinear steel-concrete composite beam element.” *J. Struct. Eng*., 126 (3), 371-381.

Ayoub, A. (2001). “A two-field mixed variational principle for partially connected composite beams.” *Finite Elements in Analysis and Design*, 37 (11), 929-959.

Batista, J., Sousa, M. (2013). “Exact finite elements for multi-layered composite beam-columns with partial interaction.” *Comput Struct*; 123:48–57.

Belarbi, A., Hsu, TTC. (1994). “Constitutive laws of concrete in tension and reinforcing bars stiffened by concrete.” *Struct J Amer Concrete Institute*; 91(4):465–74.

Chakrabarti, A., Sheikh, A., Griffith, M., Oehlers, D. (2012). “Analysis of composite beams with longitudinal and transverse partial interactions using higher order beam theory.” *Int. J. Mech. Sci*. 59; 115–125.

Challamel, N., Girhammar, U.A. (2011). “Variationally-based theories for buckling of partial composite beam–columns including shear and axial effects.” *Eng Struct* 33:2297–2319.

Das, D. (2019). “Mixed formulation for seismic analysis of shear critical reinforced concrete, steel and composite structures.” Doctoral Thesis; City, University of London.

De Veubeke, B. F. (1965). “Displacement and equilibrium models in the finite element method.” *Stress Analysis*, Wiley, pp. 145-197.

Eligehausen, R., Popov, E.P., and Bertero, V.V. (1983). "Local Bond Stress-Slip Relationships of Deformed Bars Under Generalized Excitations". Report No. UCB/EERC 83-23, Earthquake Engineering Research Center, University of California, Berkeley, p. 178.

Filippou, F.C., Fenves, G.L. (2004). “Methods of analysis for earthquake-resistant structures”, in: Y. Bozorgnia, V.V. Bertero (Eds.), Earthquake Engineering, From Engineering Seismology to Performance-Based Engineering, CRC Press LLC.

Filippou, F.C., Popov, E.P., and Bertero, V.V. (1983). "Effects of Bond Deterioration on Hysteretic Behavior of Reinforced Concrete Joints". Report No. UCB/EERC-83/19, Earthquake Engineering Research Center, University of California, Berkeley, 191 pp.

Hjiaj, M., Battini, J.-M., Nguyen, Q.H. (2012). “Large displacement analysis of shear deformable composite beams with interlayer slips.” *Int. J. Non-Linear Mech*. 47; 895–904.

Hsu, T.T.C., and Zhu, R. H. (2001). “Softened Membrane Model for Reinforced Concrete Elements in Shear” *Structural Journal, American Concrete Institute*, Vol 99, No 4, pp.460-469.

Keo, P., Nguyen, Q-H., Somja, H., Hjiaj, M. (2016). “Derivation of the exact stiffness matrix of shear-deformable multi-layered beam element in partial interaction.” *Finite Elements in Analysis and Design*, 112, 40-49.

Klinkel, S., Govindjee, S. (2002). “Using finite strain 3D-material models in beam and shell elements.” *Eng Comput* 19:902–921.

Kupfer, H. B., Hildorf, H. K., & Rusch, H. (1969). “Behavior of concrete under biaxial stresses.” *Structural Journal, American Concrete Institute*, 66(8), 656–666.

Lee, C-L., and Filippou, F. C. (2015). “Frame Element with Mixed Formulations for Composite and RC Members with Bond Slip. I: Theory and Fixed-End Rotation.” *J. Struct. Eng*., DOI: 10.1061/ (ASCE) ST.1943-541X.0001273.

Liang, Q. Q., Uy, B., Bradford, M. A., and Ronagh, H. R. (2005). “Strength analysis of steel-concrete composite beams in combined bending and shear.” *J. Struct. Eng.*, 131(10), 1593–1600.

Liu, X., Bradford, M.A., Chen, Q-J., Ban, H. (2016). “Finite element modelling of steel-concrete composite beams with high-strength friction-grip bolt shear connectors.” Finite Elements in Analysis and Design, 108 (1), 54-65.

Martinelli, E., Nguyen, Q.H., Hjiaj, M. (2012). “Dimensionless formulation and comparative study of analytical models for composite beams in partial interaction.” *J. Constr. Steel Res*. 75(0); 21–31.

Menegotto, M. and Pinto, P. E. (1973). “Method of Analysis for Cyclically Loaded Reinforced Concrete Plane Frames Including Changes in Geometry and Non-Elastic Behavior of Elements under Combined Normal Force and Bending.” *IABSE Symposium on Resistance and Ultimate Deformability of Structures Acted on by Well Defined Repeated Loads*, Lisbon.

Mullapudi, T., Ayoub, A. (2010). “Modeling of the seismic behavior of shear-critical reinforced concrete columns.” *Eng Struct*; 32(11):3601–15.

Nguyen, Q.-H., Hjiaj, M., Lai, V.-A. (2014). “Force-based FE for large displacement inelastic analysis of two-layer Timoshenko beams with interlayer slips.” *Finite Elem. Anal. Des*. 85; 1–10.

Nie, J., Xiao, Y., Chen, L. (2004). “Experimental Studies on Shear Strength of Steel–Concrete Composite Beams.” *Journal of Structural Engineering*, ASCE; vol. 130; No. 8; 1206–13.

Santos, H.A.F.A., Silberschmidt, V.V. (2014). “Hybrid equilibrium finite element formulation for composite beams with partial interaction.” *Comput. Struct*., 108, 646–656.

Saritas, A., and Filippou, F. C. (2009). “Frame element for metallic shear-yielding members under cyclic loading.” *J. Struct. Eng*. 135 (9): 1115–1123.

Schnabl, S., Saje, M., Turk, G., Planinc, I. (2007). “Locking-free two-layer Timoshenko beam element with interlayer slip.” *Finite Elem. Anal. Des*. 43; 705–714.

Silva, A.R., Sousa, J.B.M. (2009). “A family of interface elements for the analysis of composite beams with interlayer slip.” *Finite Elements in Analysis and Design* 45 (5); 305–314.

Simo, J. C. and Hughes, T. J. R. (1998). “Computational Inelasticity.” New York, Springer-Verlag.

Spacone, E., and El-Tawil, S. (2004). “Nonlinear analysis of steel-concrete composite structures: State of the art.” *J. Struct. Eng*., 10.1061/(ASCE) 0733-9445(2004)130:2(159), 159–168.

Taig, G., Ranzi, G., Dias-da-Costa, D., Piccardo, G., and Luongo, A. (2015). “A GBT Model for the Analysis of Composite Steel–Concrete Beams with Partial Shear Interaction.” *Structures*; 4:27–37.

Uddin, M-A., Sheikh, A., Brown, D., Bennett, T., Uy, B. (2018). “Geometrically nonlinear inelastic analysis of steel–concrete composite beams with partial interaction using a higher-order beam theory.” *Int. J. Non-Linear Mech*. 100; 34–47.

Vasdravellis, G. and Uy, B. (2014), “Shear strength and moment-shear interaction in steel-concrete composite beams”, J. Struct. Eng., 140(11), 04014084.

Vecchio, F. J. (1992). “Finite element modeling of concrete expansion and confinement.” *Journal of Structural Engineering*, ASCE, 118(9), 2390–2405.

Zhu, RRH., Hsu, TTC., Lee, JY. (2001). “Rational shear modulus for smeared crack analysis of reinforced concrete.” *Struct J Amer Concrete Institute*; 98(4):443–50.

Zhu, RRH., Hsu, TTC. (2002). “Poisson effect of reinforced concrete membrane elements.” *Struct J Amer Concrete Institute*; 99(5):631–40.

Zienkiewicz, O. C., and Taylor, R. L. (1989). “The finite element method. Vol. 1, Basic formulation and linear problems”, McGraw-Hill, London.

Zona, A., Ranzi, G. (2011). “Finite element models for nonlinear analysis of steel– concrete composite beams with partial interaction in combined bending and shear.” *Finite Elem. Anal. Des.* 47(2); 98–118.

Zulfiqar, N., and Filippou, F.C. (1990). "Models of Critical Regions in Reinforced Concrete Frames under Seismic Excitations". Report No. UCB/EERC-90/06, Earthquake Engineering Research Center, University of California, Berkeley.

Table 1. State Determination Process – Mixed Formulation

Step 1: Determine the incremental structural nodal displacement and its update with respect to global axes of reference by the solver:

$\Delta \boldsymbol{U}^{i+1} = \left[\boldsymbol{K}^{i}\right]^{-1}(\boldsymbol{P}^{k+1} - \boldsymbol{P}_{R}^{i})$ (By the solver)

Where

$\boldsymbol{P}^{k+1} = \boldsymbol{P}^{k} + \Delta \boldsymbol{P}^{k+1}$ (Update of applied load vector)

$\boldsymbol{U}^{i+1} = \boldsymbol{U}^{i} + \Delta \boldsymbol{U}^{i+1}$ (Update of global nodal displacement vector)

Step 2: Determine the incremental element nodal deformation and its update with respect to the basic axes of reference with the help of nodal compatibility and extraction of rigid body modes:

$\Delta \boldsymbol{u}_{\boldsymbol{IJ}_{\boldsymbol{ele}}}^{\boldsymbol{i+1}} = \boldsymbol{A}_{\boldsymbol{IJ}} \Delta \boldsymbol{U}^{i+1}$ (By the solver)

Where A_{IJ} is the structural compatibility matrix.

$\Delta \boldsymbol{v}^{i+1} = \boldsymbol{a}_{\boldsymbol{c}} \Delta \boldsymbol{u}_{\boldsymbol{IJ}_{\boldsymbol{ele}}}^{\boldsymbol{i+1}}$ (By Element Subroutine)

$\boldsymbol{v}^{i+1} = \boldsymbol{v}^{i} + \Delta \boldsymbol{v}^{i+1}$ (Update of element nodal deformation vector)

Step 3: Determine the incremental element nodal force and its update with respect to the basic axes of reference for a given element nodal deformation vector which remains constant for element iteration loop counter j:

$\Delta \boldsymbol{q}^{j} = \boldsymbol{k}_{\boldsymbol{ele}}^{\boldsymbol{j-1}}(\boldsymbol{G} \Delta \boldsymbol{v}^{i+1} - \boldsymbol{u}^{r,j-1})$

$\boldsymbol{q}^{j+1} = \boldsymbol{q}^{j} + \Delta \boldsymbol{q}^{j}$ (Update of element nodal force vector)

Step 4: Determine the incremental section deformation and slip and its update with respect to the basic axes of reference for a given element nodal force vector:

$\Delta \boldsymbol{d}^{j} = \left[\boldsymbol{k}_{\boldsymbol{sec}}^{\boldsymbol{j-1}}\right]^{-1}(\boldsymbol{b} \Delta \boldsymbol{q}^{j})$

$\boldsymbol{d}^{j+1} = \boldsymbol{d}^{j} + \Delta \boldsymbol{d}^{j}$ (Update of section deformation vector)

$\boldsymbol{q}_{\boldsymbol{sec}}{}^{j+1} = \boldsymbol{q}_{\boldsymbol{sec}}{}^{j} + (\boldsymbol{b} \Delta \boldsymbol{q}^{j})$ (Update of section force vector)

$\Delta \boldsymbol{s}^{i} = \boldsymbol{B}_{\boldsymbol{b}}(x) \Delta \boldsymbol{v}^{i+1}$

$\boldsymbol{s}^{i+1} = \boldsymbol{s}^{i} + \Delta \boldsymbol{s}^{i}$ (Update of slip)

Step 5: Determine the section tangent stiffness ($\boldsymbol{k}_{\boldsymbol{sec}}^{\boldsymbol{j+1}}$) and resistance vector ($\boldsymbol{p}_{\boldsymbol{sec}}^{\boldsymbol{j+1}}$) for a given section deformation vector with mid-point integration rule and material state determination. Also, determine bond forces $\tau_{x}^{b,i+1}$ and bond stiffness $\boldsymbol{K}_{\boldsymbol{b}}{}^{\boldsymbol{i+1}}$ from the bond constitutive relations.

Step 6: Determine the element residual deformation and flexibility matrix and update the element nodal forces with updated section deformation and forces for the next element iteration until the norm of element nodal energy becomes less than the specified tolerance value to dissipate the element residual deformation:

$$\boldsymbol{f}_{\boldsymbol{ele}}^{\boldsymbol{j+1}} = \sum \boldsymbol{b}^{\boldsymbol{T}} \left[\boldsymbol{k}_{\boldsymbol{sec}}^{\boldsymbol{j+1}}\right]^{-\boldsymbol{1}} \boldsymbol{b}$$

$$\boldsymbol{u}^{r,j+1} = \boldsymbol{u}^{r,j} + \sum \boldsymbol{b}^{\boldsymbol{T}} \left[\boldsymbol{k}_{\boldsymbol{sec}}^{\boldsymbol{j+1}}\right]^{-\boldsymbol{1}} (\boldsymbol{q}_{\boldsymbol{sec}}{}^{j+1} - \boldsymbol{p}_{\boldsymbol{sec}}^{\boldsymbol{j+1}})$$(Update of element nodal residual deformation vector)

$$\boldsymbol{q}^{j+2} = \boldsymbol{q}^{j+1} - \left[\boldsymbol{f}_{\boldsymbol{ele}}^{\boldsymbol{j+1}}\right]^{-1} \boldsymbol{u}^{r,j+1}$$

$$\boldsymbol{d}^{j+2} = \boldsymbol{d}^{j+1} + \left[\boldsymbol{k}_{\boldsymbol{sec}}^{\boldsymbol{j+1}}\right]^{-\boldsymbol{1}} \left(\boldsymbol{q}_{\boldsymbol{sec}}{}^{j+1} - \boldsymbol{p}_{\boldsymbol{sec}}^{\boldsymbol{j+1}}\right) - \left[\boldsymbol{k}_{\boldsymbol{sec}}^{\boldsymbol{j+1}}\right]^{-\boldsymbol{1}} (\boldsymbol{b}\left[\boldsymbol{f}_{\boldsymbol{ele}}^{\boldsymbol{j+1}}\right]^{-1} \boldsymbol{u}^{r,j+1})$$

$$\boldsymbol{q}_{\boldsymbol{sec}}{}^{j+2} = \boldsymbol{q}_{\boldsymbol{sec}}{}^{j+1} - \ (\boldsymbol{b}\left[\boldsymbol{f}_{\boldsymbol{ele}}^{\boldsymbol{j+1}}\right]^{-1} \boldsymbol{u}^{r,j+1})$$

Step 7: Determine the element stiffness matrix and resistance vector in iteration counter *i* for the given nodal element deformation upon the convergence of element compatibility at the basic frame of reference:

$$\boldsymbol{K}_{\boldsymbol{ele}}^{\boldsymbol{i+1}} = \boldsymbol{K}_{\boldsymbol{c+s}}^{\boldsymbol{i+1}} + \boldsymbol{K}_{\boldsymbol{B}}^{\boldsymbol{i+1}}$$

$$\boldsymbol{K}_{\boldsymbol{c+s}}^{\boldsymbol{i+1}} = \boldsymbol{G}^{\boldsymbol{T}}\left[\boldsymbol{f}_{\boldsymbol{ele}}^{\boldsymbol{j+1}}\right]^{-1} \boldsymbol{G}$$

$$\boldsymbol{K}_{\boldsymbol{B}}^{\boldsymbol{i+1}} = \sum \boldsymbol{B}_{\boldsymbol{b}}{}^{\boldsymbol{T}} \boldsymbol{K}_{\boldsymbol{b}}{}^{\boldsymbol{i+1}} \boldsymbol{B}_{\boldsymbol{b}}$$

$$\boldsymbol{P}^{\boldsymbol{r,i+1}} = \boldsymbol{P}_{\boldsymbol{c+s}}^{\boldsymbol{r,i+1}} + \ \boldsymbol{P}_{\boldsymbol{b}}^{\boldsymbol{r,i+1}}$$

$$\boldsymbol{P}_{\boldsymbol{c+s}}^{\boldsymbol{r,i+1}} = \boldsymbol{G}^{\boldsymbol{T}} \boldsymbol{q}_{\boldsymbol{ele}}^{\boldsymbol{i+1}}$$

$$\boldsymbol{P}_{\boldsymbol{b}}^{\boldsymbol{r,i+1}} = \sum \boldsymbol{B}_{\boldsymbol{b}}{}^{T} \tau_{x}^{b,i+1}$$

Step 8: Determine the element stiffness matrix and resistance vector in iteration counter *i* at the global frame of reference:

$$\boldsymbol{K}_{\boldsymbol{ele,glo}}^{\boldsymbol{i+1}} = \boldsymbol{a}_{\boldsymbol{c}}^{\boldsymbol{T}} \boldsymbol{K}_{\boldsymbol{ele}}^{\boldsymbol{i+1}} \boldsymbol{a}_{\boldsymbol{c}}$$

$$\boldsymbol{Q}_{\boldsymbol{ele,glo}}^{\boldsymbol{i+1}} = \boldsymbol{a}_{\boldsymbol{c}}^{\boldsymbol{T}} \boldsymbol{P}^{\boldsymbol{r,i+1}}$$

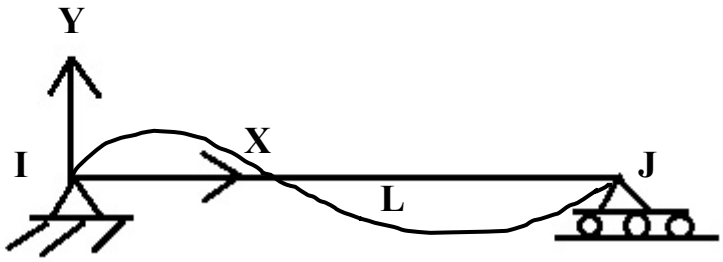

Figure 1. Basic Reference System without Rigid Body Modes

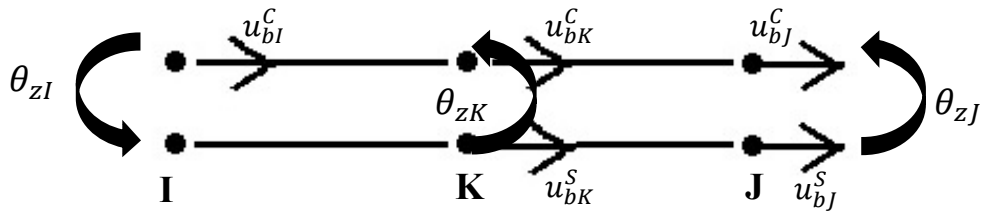

Figure 2. Element Nodal Deformations

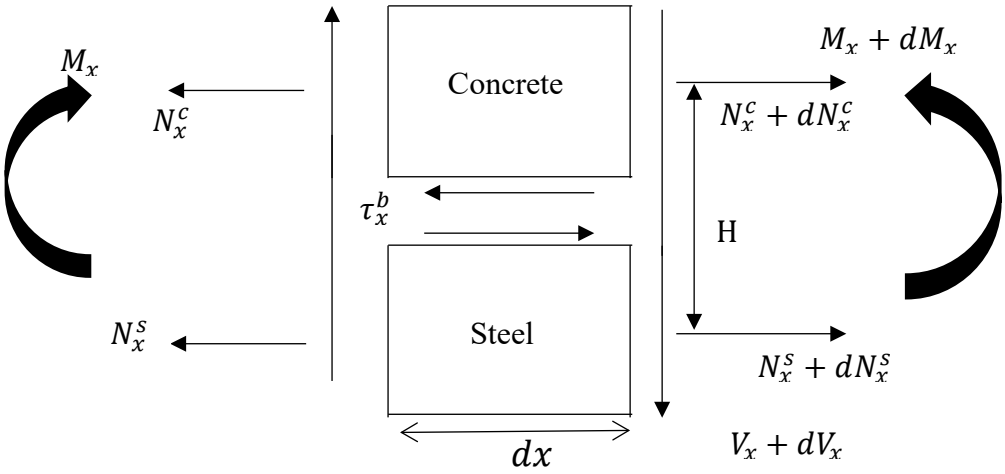

Figure 3. Section Differential Equilibrium

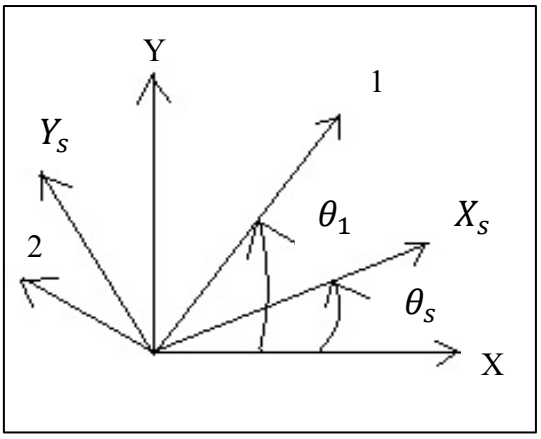

Figure 4. Applied Principal Stresses and Reinforcement Directions of RC Element

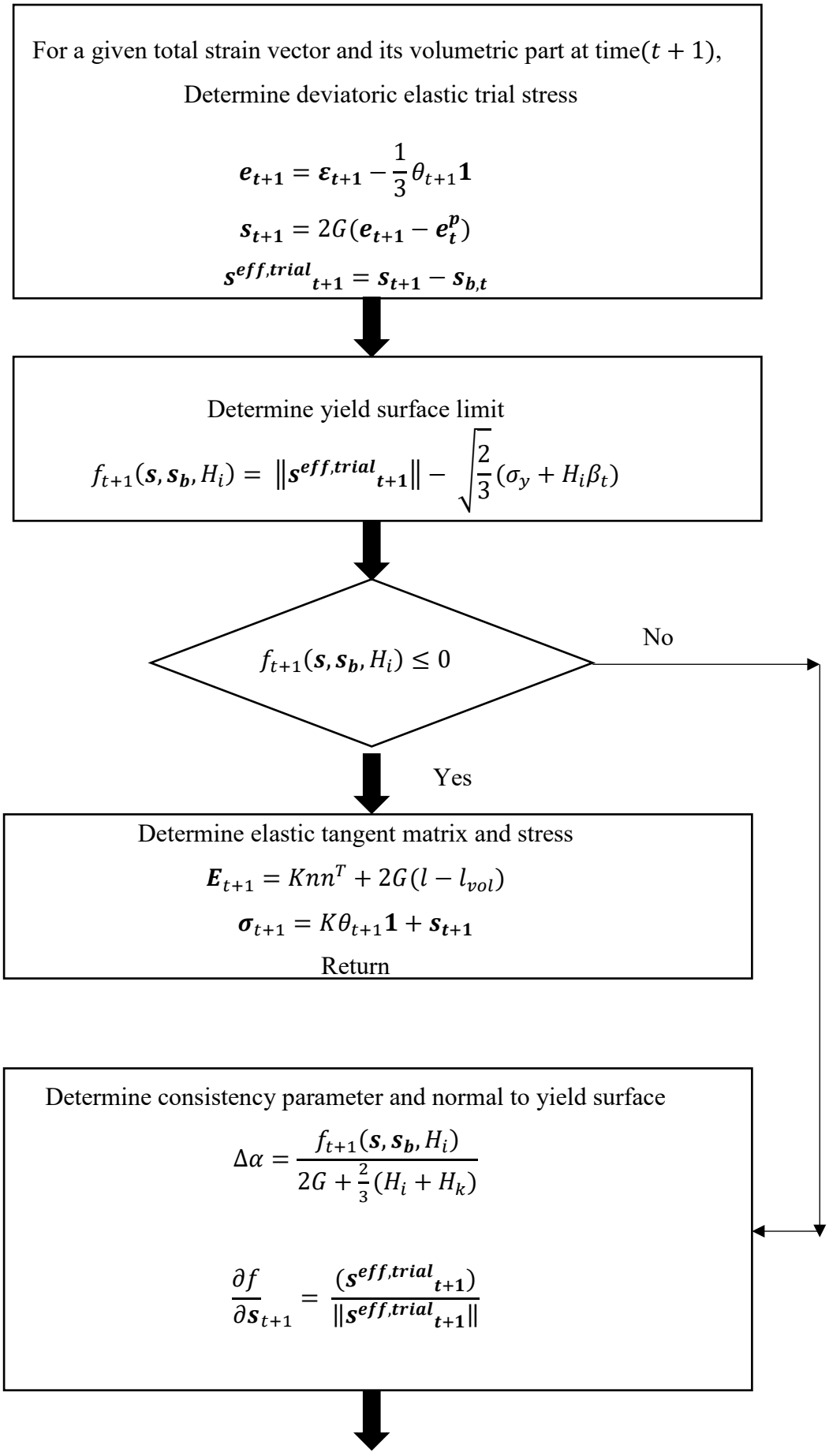
For a given total strain vector and its volumetric part at time$(t+1)$,
Determine deviatoric elastic trial stress
$\boldsymbol{e_{t+1}} = \boldsymbol{\varepsilon_{t+1}} - \frac{1}{3}\theta_{t+1}\mathbf{1}$
$\boldsymbol{s_{t+1}} = 2G(\boldsymbol{e_{t+1}} - \boldsymbol{e_t^p})$
$\boldsymbol{s^{eff,trial}}_{t+1} = \boldsymbol{s_{t+1}} - \boldsymbol{s_{b,t}}$
Determine yield surface limit
$f_{t+1}(\boldsymbol{s}, \boldsymbol{s_b}, H_i) = \left\|\boldsymbol{s^{eff,trial}}_{t+1}\right\| - \sqrt{\frac{2}{3}}(\sigma_y + H_i\beta_t)$
$f_{t+1}(\boldsymbol{s}, \boldsymbol{s_b}, H_i) \leq 0$
No
Yes
Determine elastic tangent matrix and stress
$\boldsymbol{E}_{t+1} = Knn^T + 2G(l - l_{vol})$
$\boldsymbol{\sigma}_{t+1} = K\theta_{t+1}\mathbf{1} + \boldsymbol{s_{t+1}}$
Return
Determine consistency parameter and normal to yield surface
$\Delta\alpha = \frac{f_{t+1}(\boldsymbol{s}, \boldsymbol{s_b}, H_i)}{2G + \frac{2}{3}(H_i + H_k)}$
$\frac{\partial f}{\partial \boldsymbol{s}_{t+1}} = \frac{(\boldsymbol{s^{eff,trial}}_{t+1})}{\|\boldsymbol{s^{eff,trial}}_{t+1}\|}$

Determine the updated hardening variable, plastic strain and back stress

$$\beta_{t+1} = \beta_t + \sqrt{\frac{2}{3}}\Delta\alpha$$

$$\boldsymbol{e}^{\boldsymbol{p}}_{\boldsymbol{t+1}} = \boldsymbol{e}^{\boldsymbol{p}}_{\boldsymbol{t}} + \Delta\alpha \frac{\partial f}{\partial \boldsymbol{s}_{t+1}}$$

$$\boldsymbol{s}_{\boldsymbol{b,t+1}} = \boldsymbol{s}_{\boldsymbol{b,t}} + \frac{2}{3} H_k \Delta\alpha \frac{\partial f}{\partial \boldsymbol{s}_{t+1}}$$

Determine the stress vector and consistent elastic-plastic tangent matrix

$$\boldsymbol{\sigma}_{t+1} = K\theta_{t+1}\mathbf{1} + \boldsymbol{s}_{\boldsymbol{t+1}} - 2G\Delta\alpha \frac{\partial f}{\partial \boldsymbol{s}_{t+1}}$$

$$\boldsymbol{E}_{t+1} = K(\mathbf{1} * \mathbf{1}) + 2G\left[(1-\omega)\left(\mathrm{II} - \frac{1}{3}(\mathbf{1} * \mathbf{1})\right) - \left(\frac{\mathrm{G}}{\mathrm{G^p}} - \omega\right)\left(\frac{\partial \mathrm{f}}{\partial \mathrm{s_{t+1}}} * \frac{\partial \mathrm{f}}{\partial \mathrm{s_{t+1}}}\right)\right]$$

$$\mathrm{G^p} = G + \frac{H_i + H_k}{3}$$

$$\omega = \frac{2G\Delta\alpha}{\|\boldsymbol{s}^{\boldsymbol{eff,trial}}_{\boldsymbol{t+1}}\|}$$

Return

Figure 5. Radial Return Mapping Algorithm- J2 Plasticity

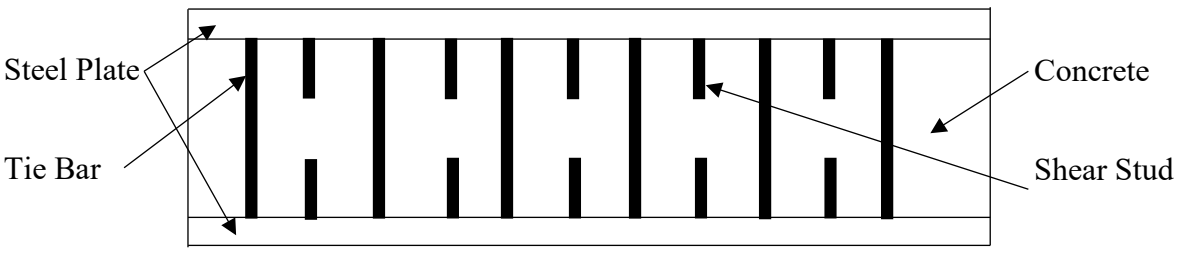

Figure 6. Geometry of Sandwiched Beam

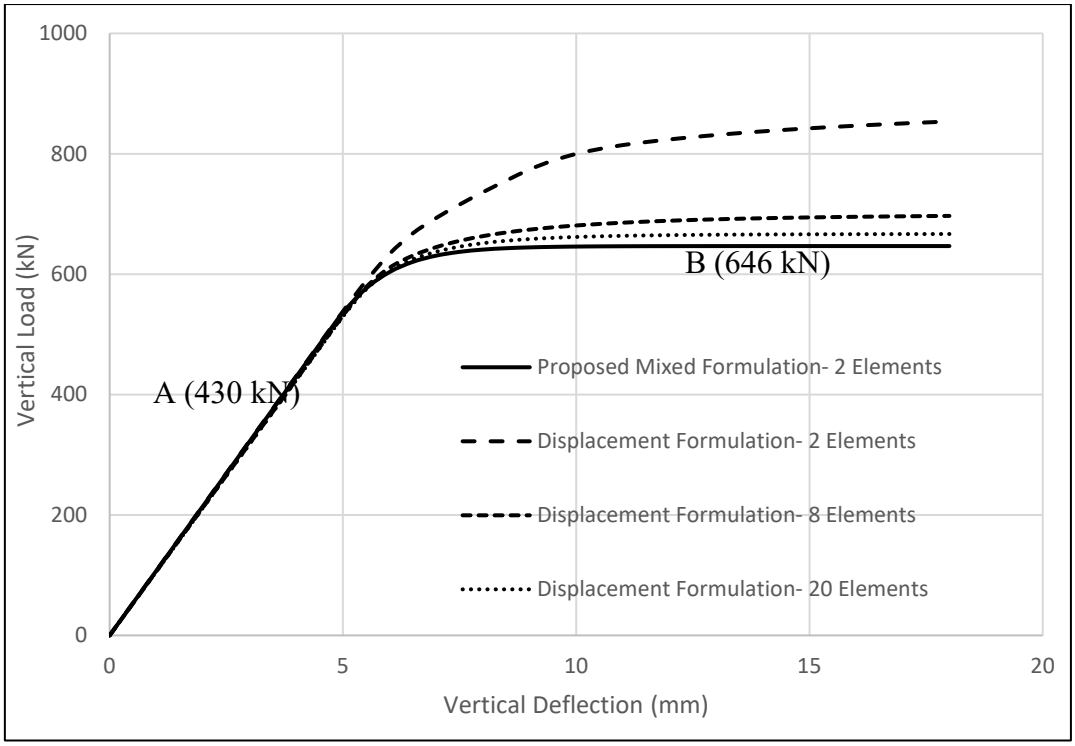

Figure 7. Load-Deflection Response

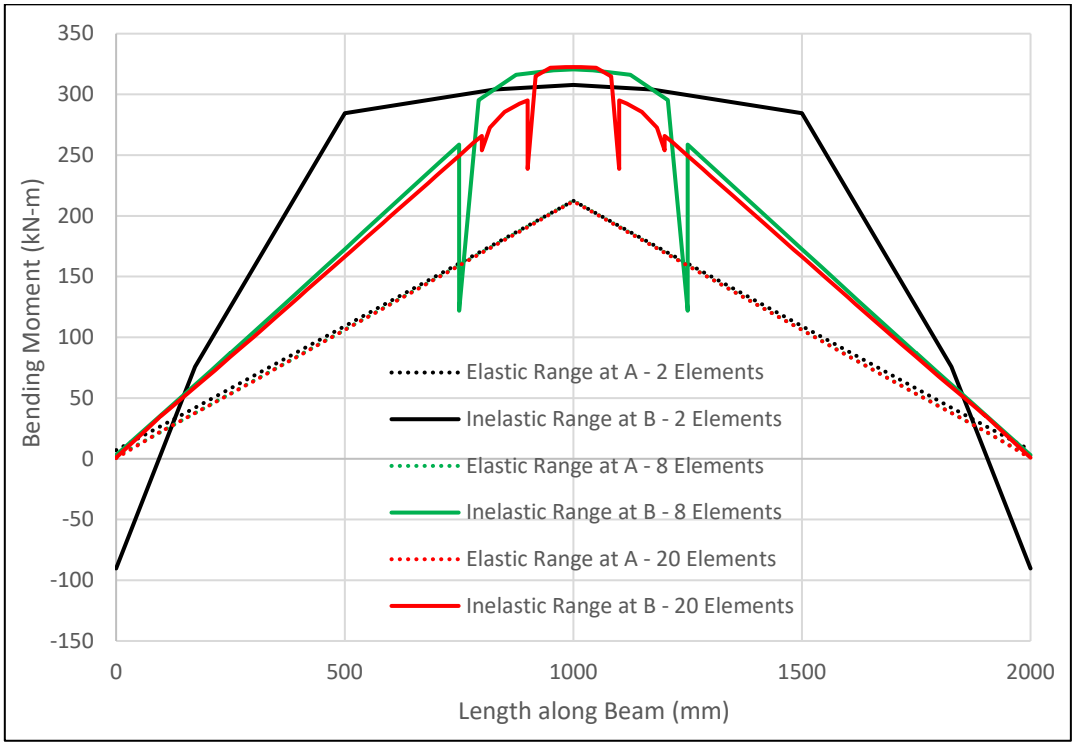

Figure 8. Bending Moment Distribution (Displacement Model)

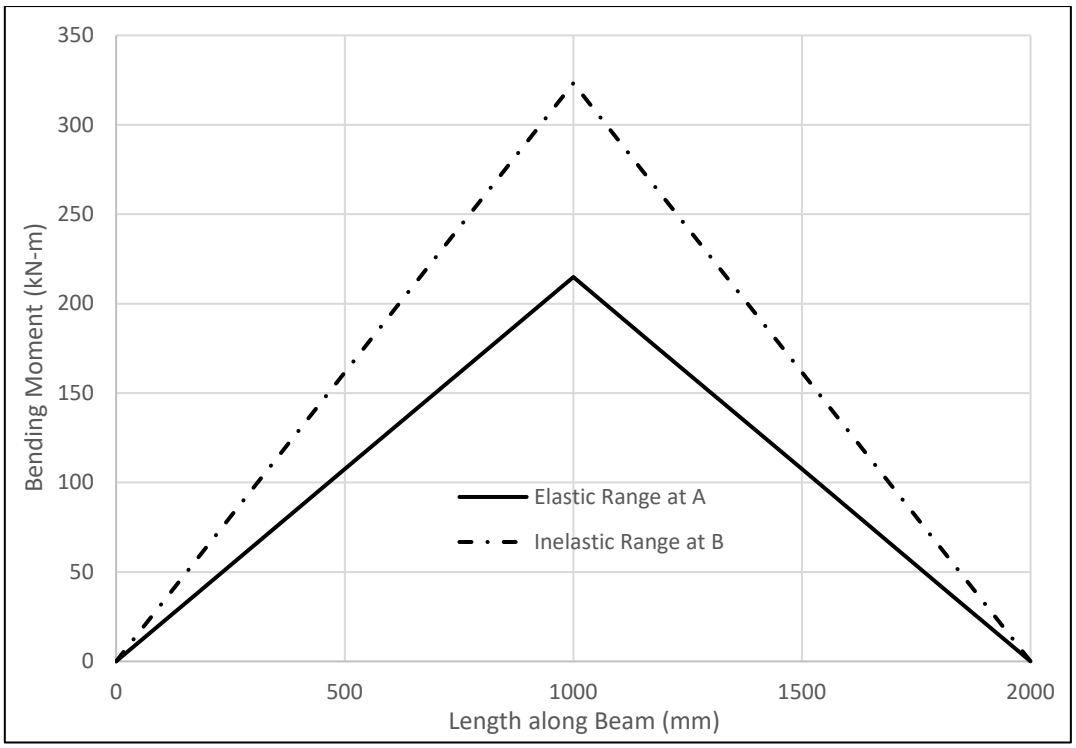

Figure 9. Bending Moment Distribution (Mixed Model)

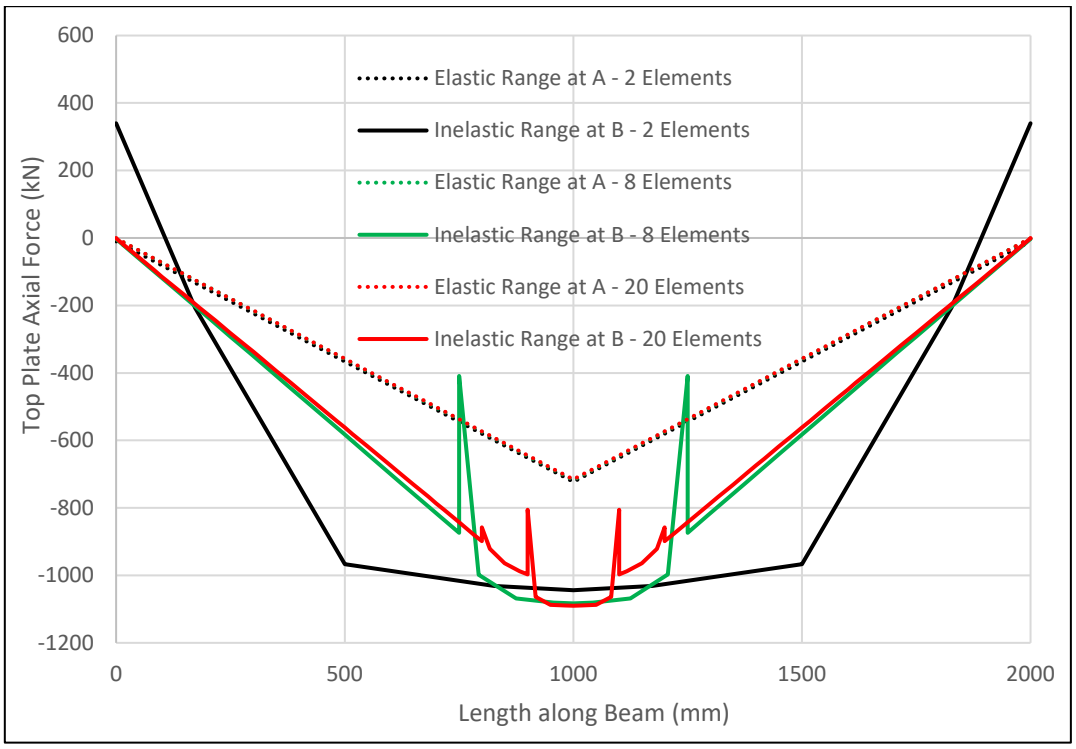

Figure 10. Top Plate Axial Force Distribution (Displacement Model)

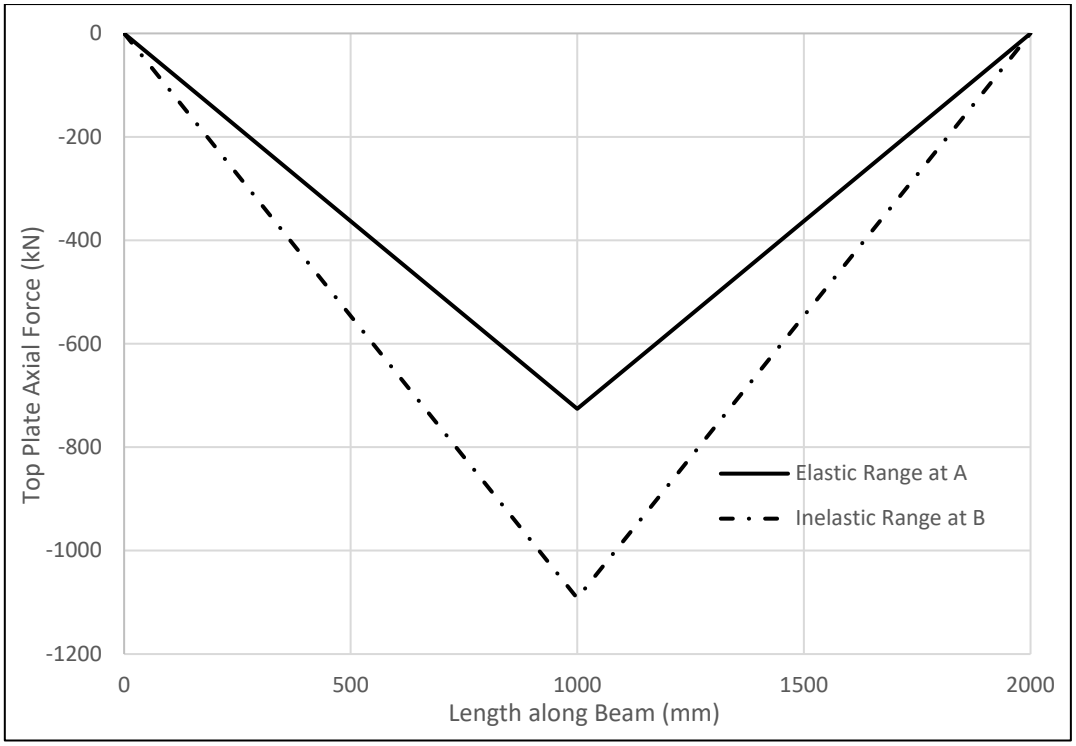

Figure 11. Top Plate Axial Force Distribution (Mixed Model)

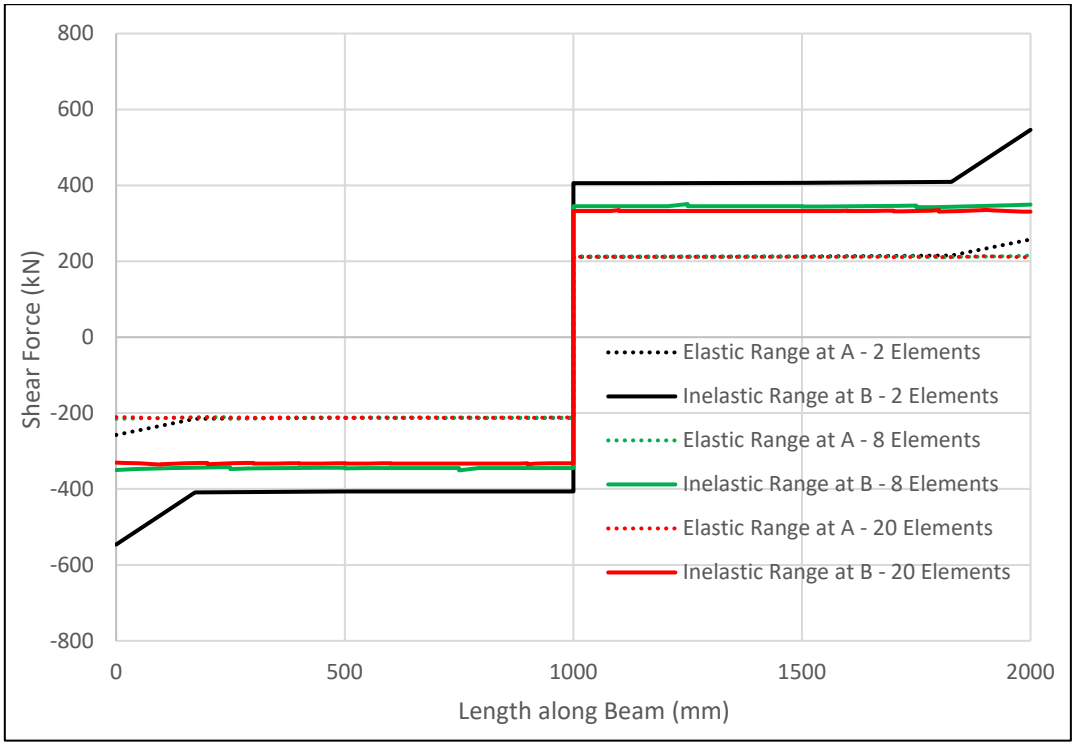

Figure 12. Shear Force Distribution (Displacement Model)

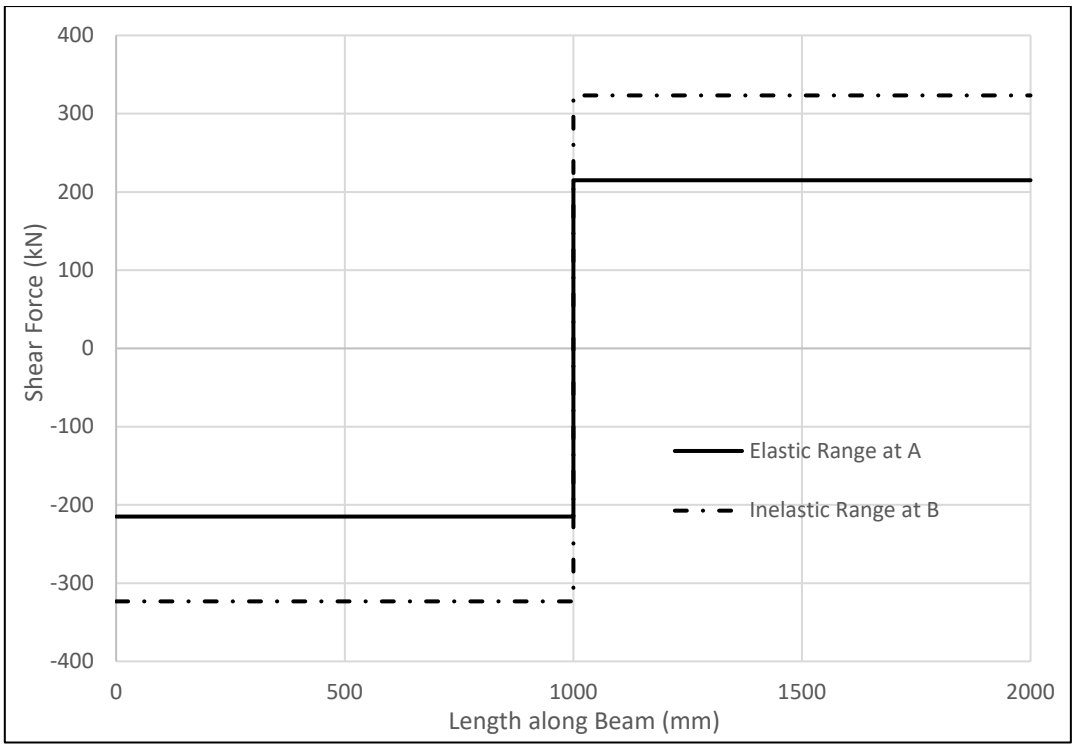

Figure 13. Shear Force Distribution (Mixed Model)

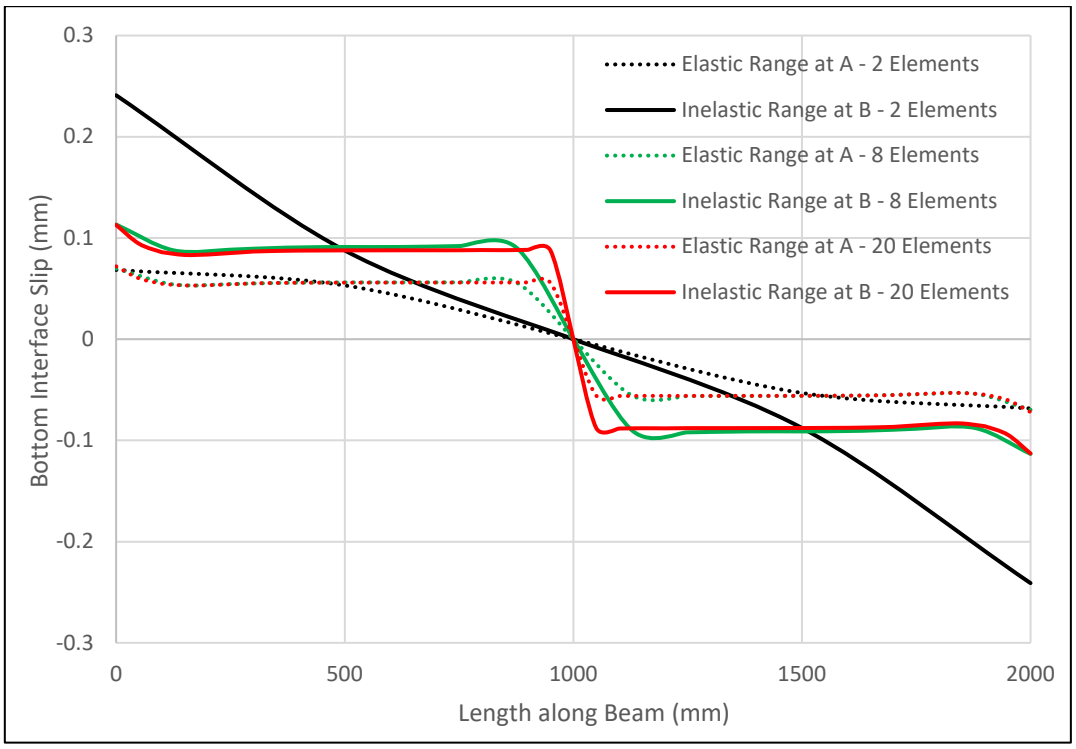

Figure 14. Bottom Interface Slip Distribution (Displacement Model)

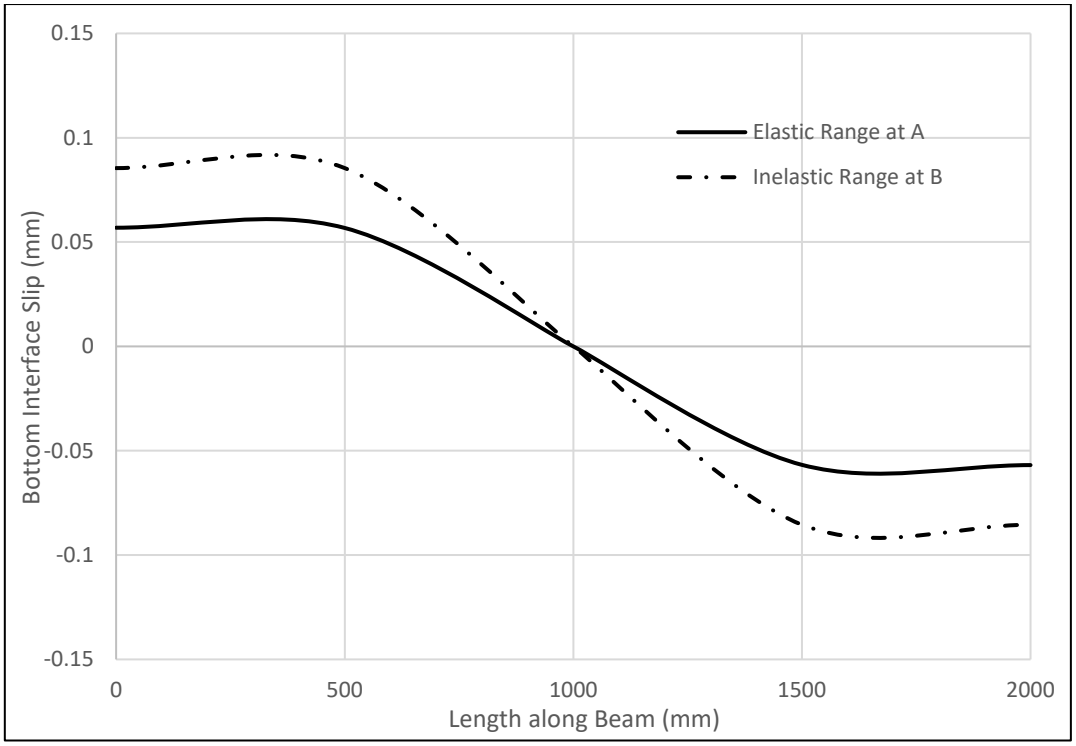

Figure 15. Bottom Interface Slip Distribution (Mixed Model)

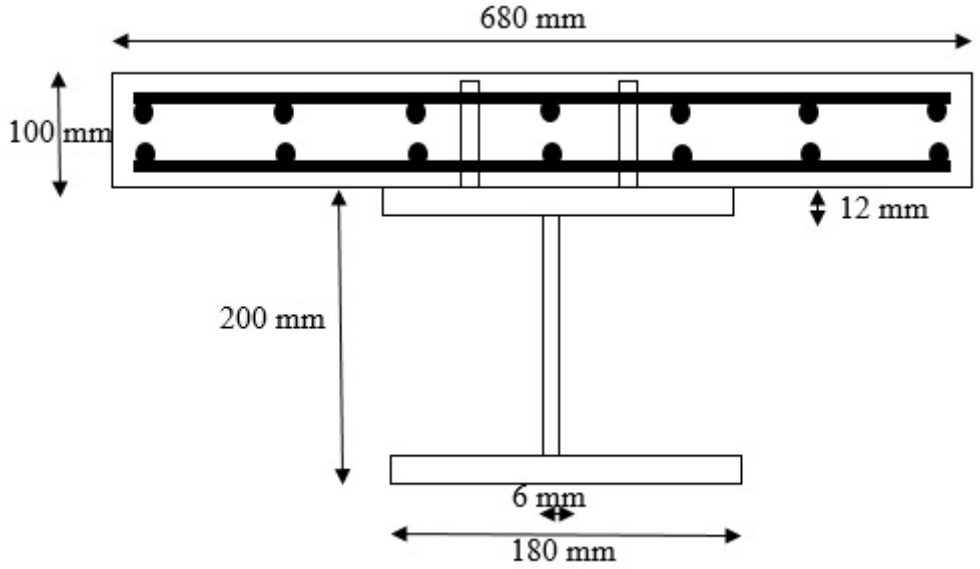

Figure 16. Cross-Section of Composite Beam CBS-2

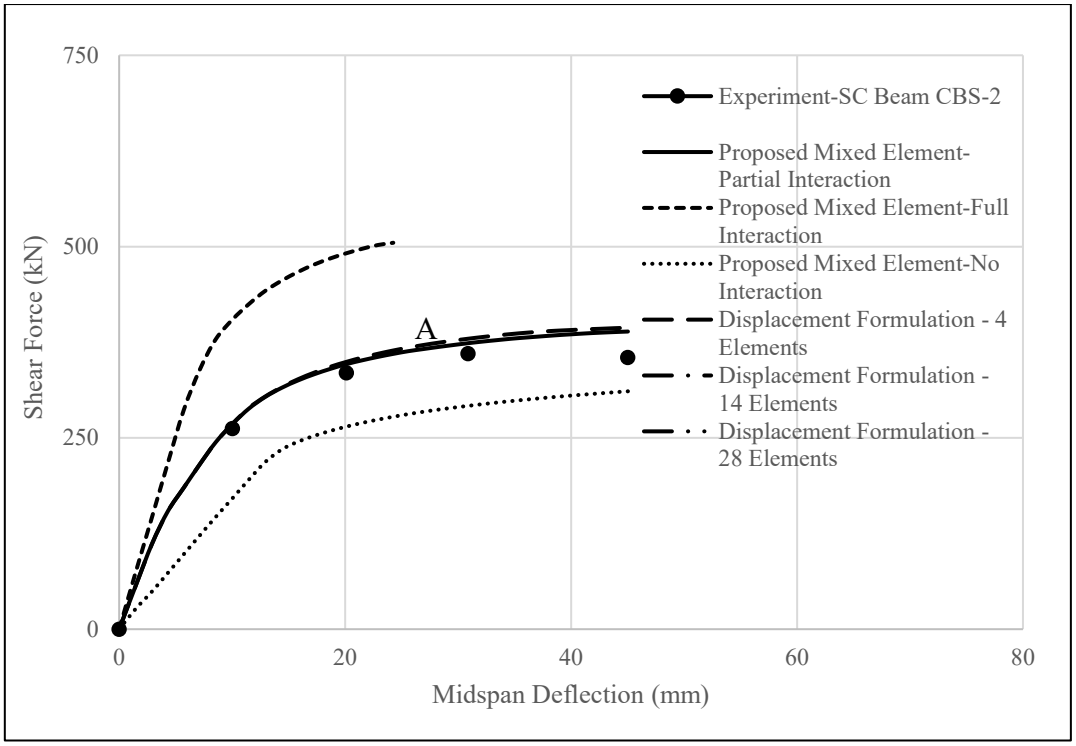

Figure 17. Load-Deflection Response of SC Beam CBS-2

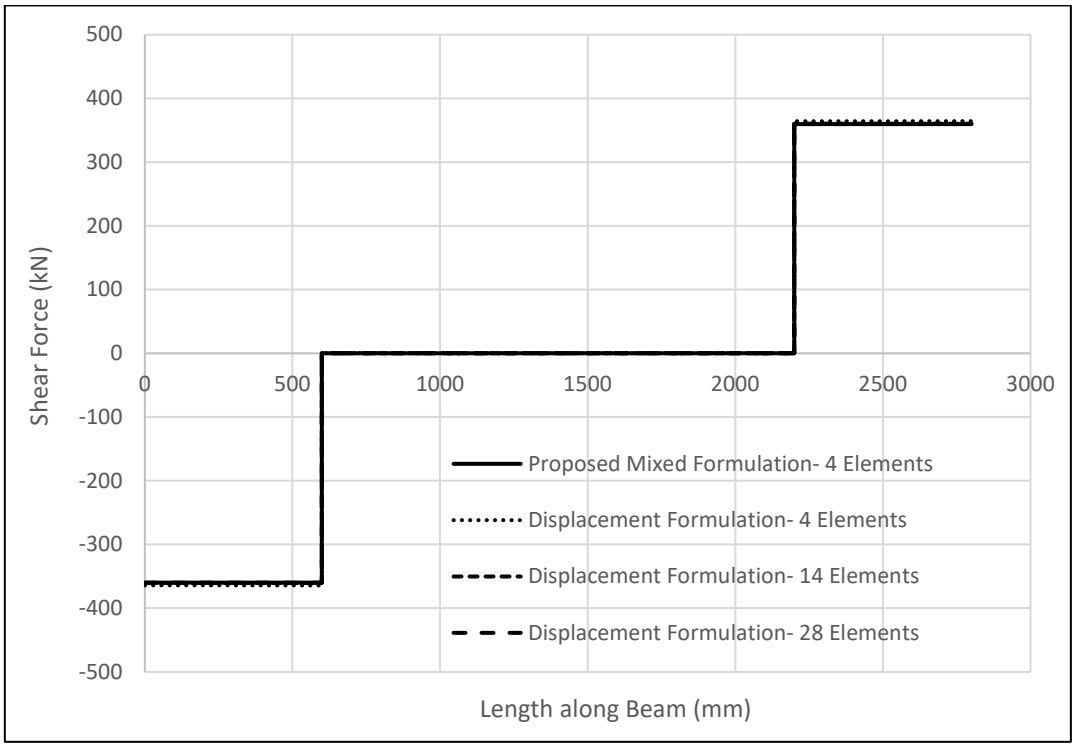

Figure 18. Shear Force Distribution along the Length of Beam

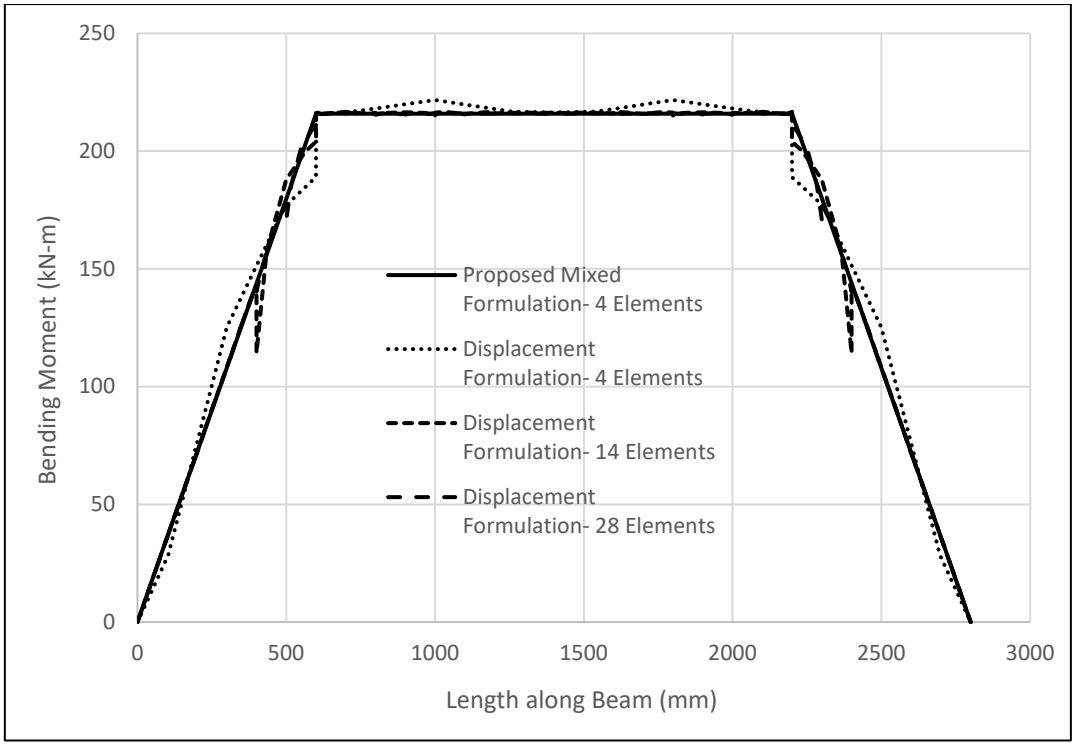

Figure 19. Bending Moment Distribution along the Length of Beam

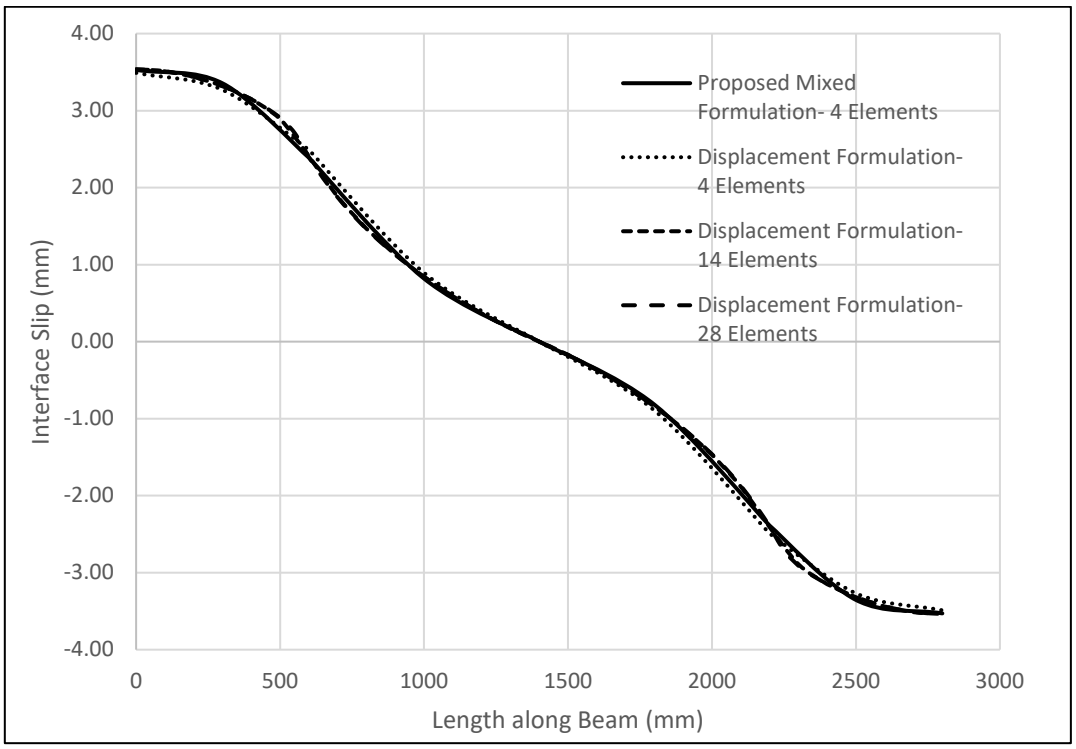

Figure 20. Interface Slip Distribution along the Length of Beam

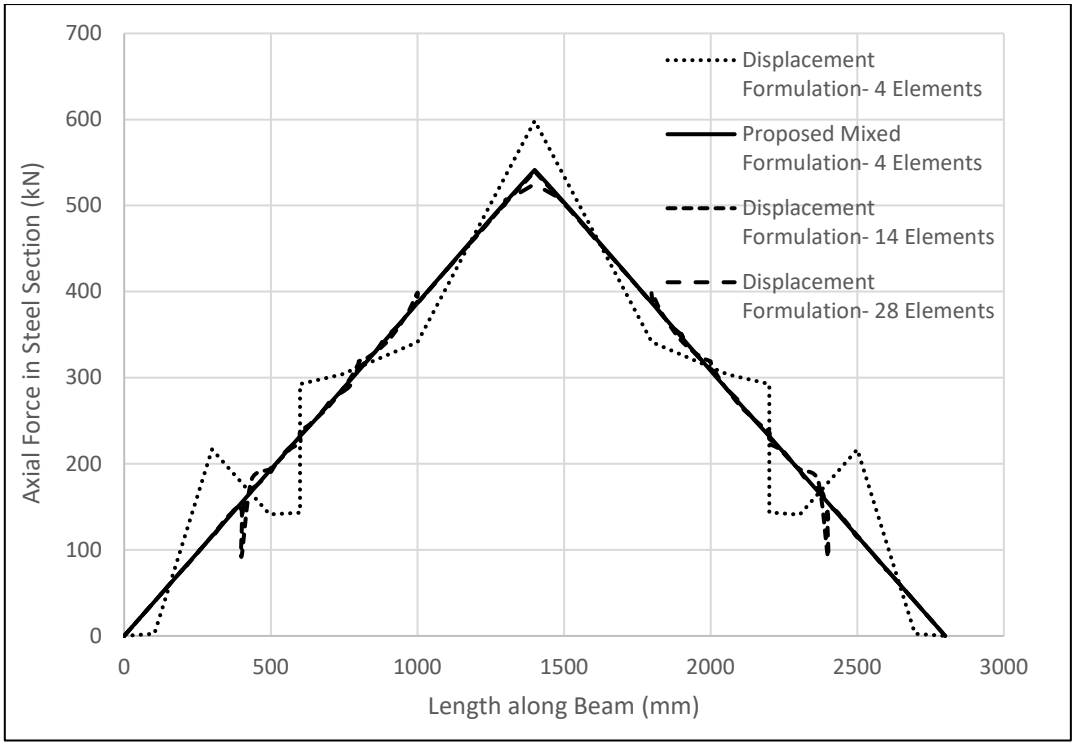

Figure 21. Axial Force Distribution along the Length of Beam in Steel Section

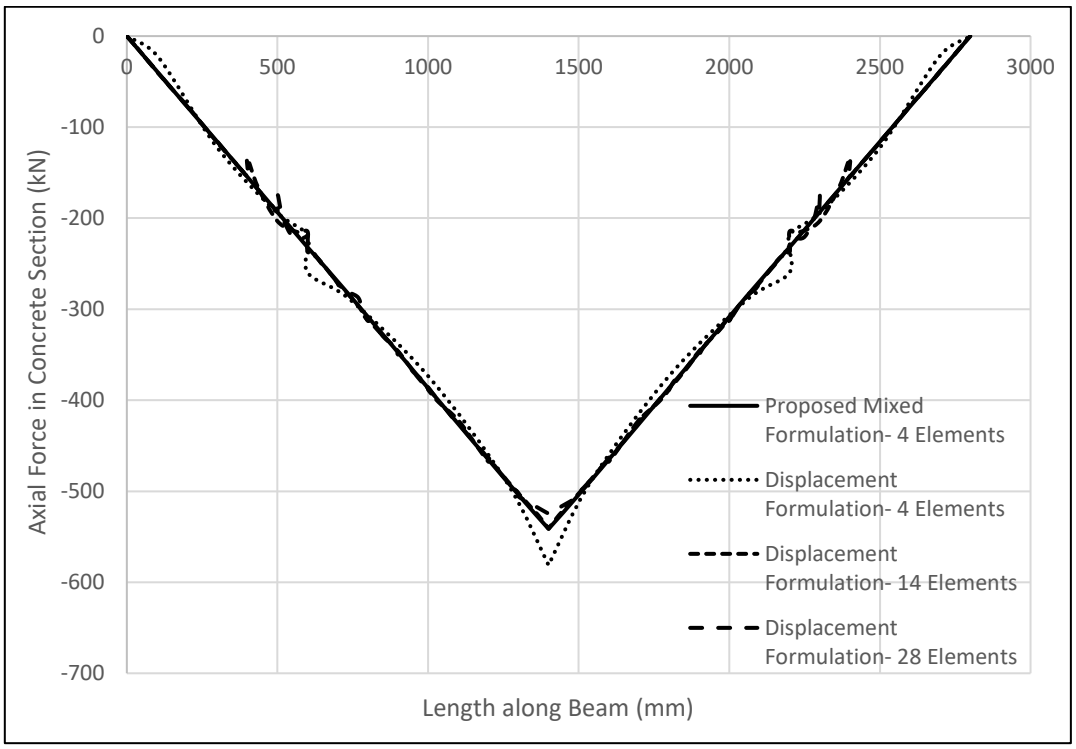

Figure 22. Axial Force Distribution along the Length of Beam in Concrete Section

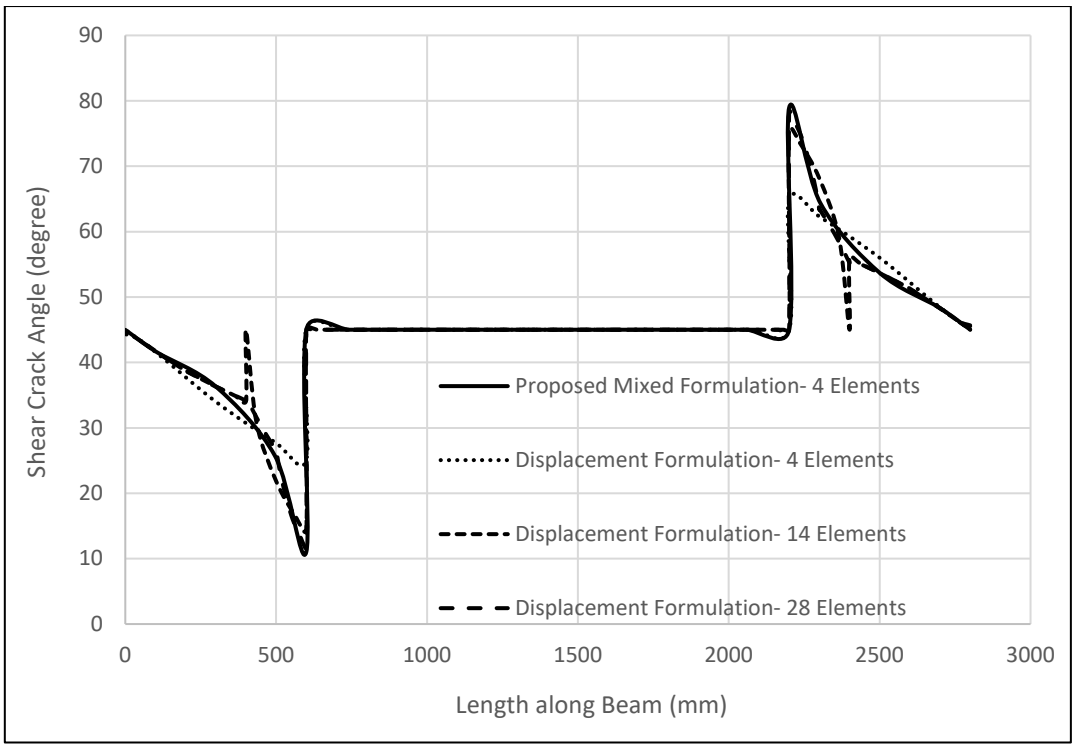

Figure 23. Applied Stress Angle Distribution along the Length of Beam in Middle Fibre of Concrete Section

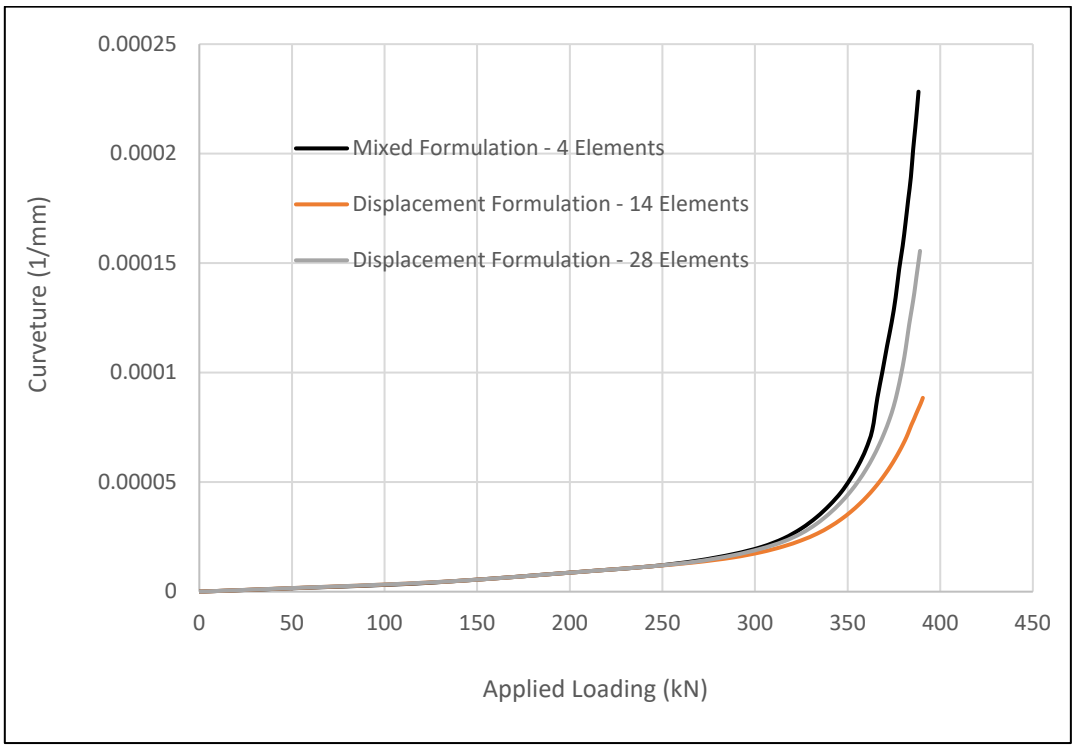

Figure 24. Curvature-Loading Response at loading point

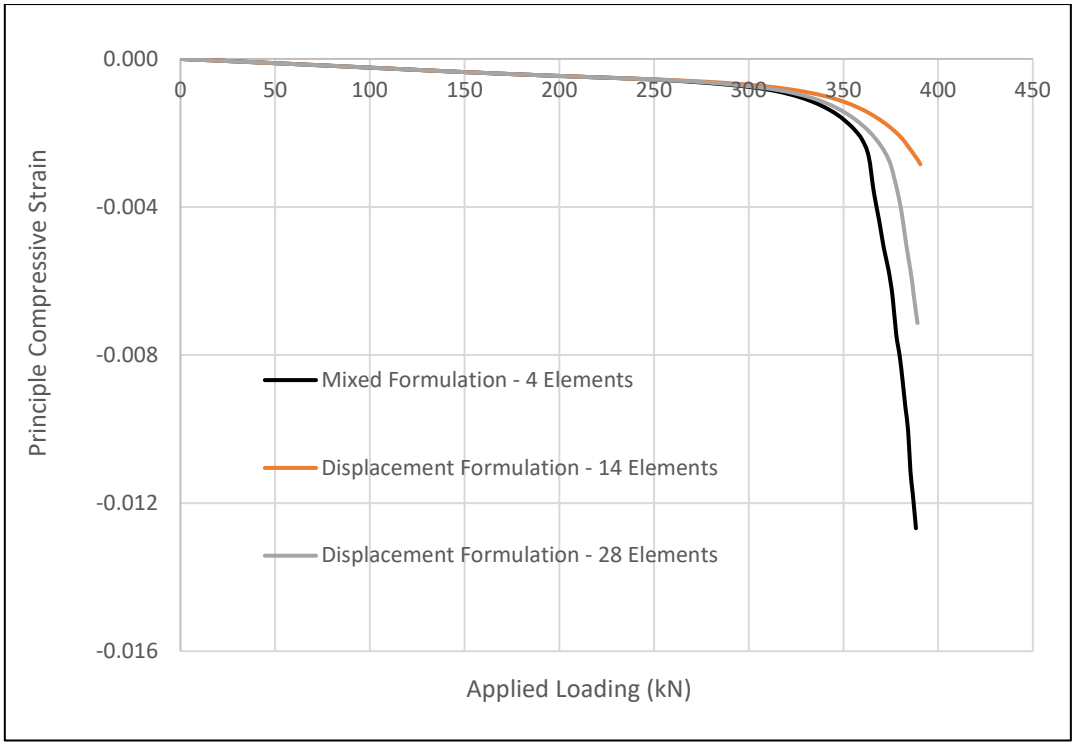

Figure 25. Principle Compressive Strain-Loading Response of top concrete fibre at loading point

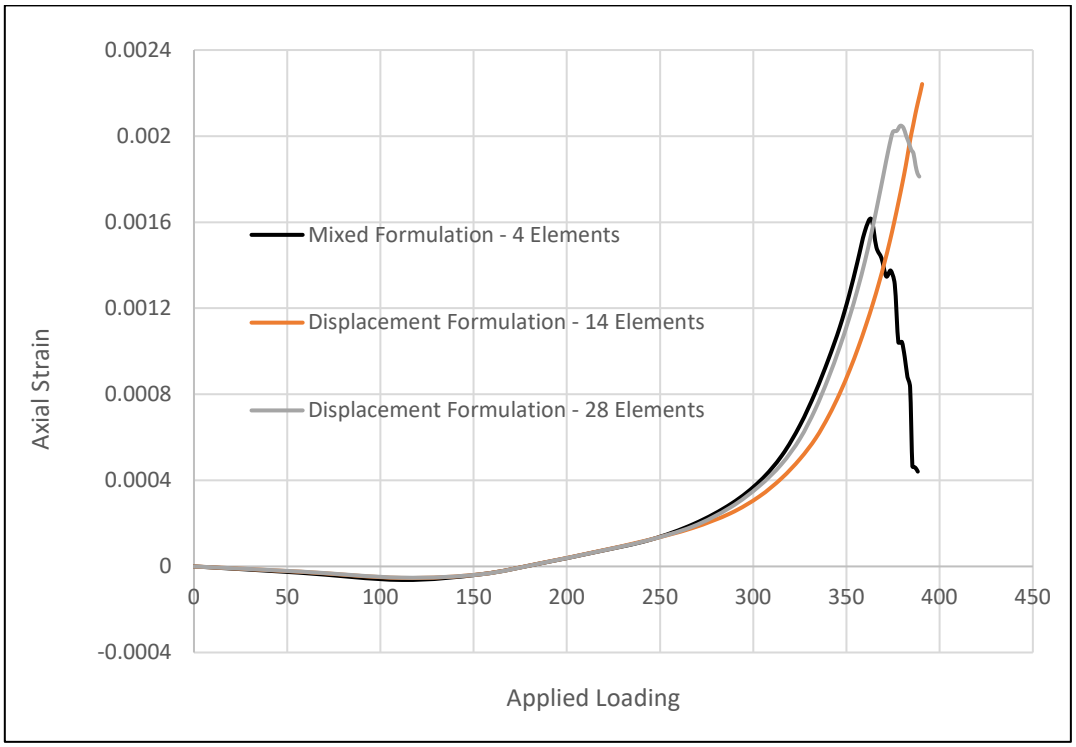

Figure 26. Axial Strain-Loading Response of bottom rebar of concrete deck at loading point

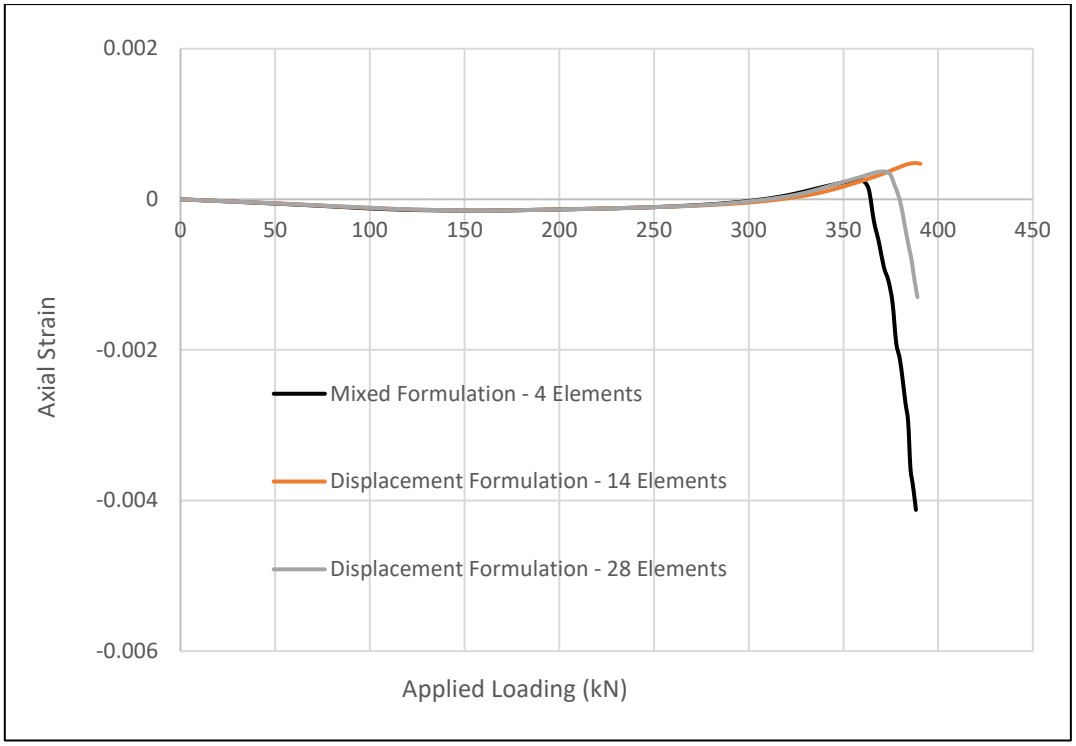

Figure 27. Axial Strain-Loading Response of top rebar of concrete deck at loading point